Optimal Regulation of Circadian Clock

by

Zhi Xian Ye

Dissertation Submitted in Partial Fulfillment of the
Requirements for the Degree of
Bachelor of Science

in the
Department of Physics
Faculty of Science

SIMON FRASER UNIVERSITY
Summer 2018

Abstract

A circadian clock (sometimes called a circadian oscillator or rhythm) oscillates roughly once every 24 hours, enabling us to organize our physical and mental activities at the time that is most optimal. The Nobel Prize in physiology or medicine in 2017 was awarded to the scientists who discovered the molecular mechanisms controlling the circadian clock.[1] In this thesis, we study the circadian clock in a physical and mathematical setting. The modified Kuramoto model which describes the synchronization between coupled oscillators is chosen as the equation of motion to study the circadian clock of living organisms. More specifically, we picture our physical system as two individual oscillators, one the solar-cycle oscillator and the other an internal-clock oscillator of a living organism. As in the real world, there is always random noise that prevents living organisms from having perfect knowledge of the outside world. Noise can either come from the environmental background or uncertainty in the internal processing of the organism. The deterministic and stochastic versions of the modified Kuramoto model are separately analyzed. The cost analysis based on the phase synchronization between the two oscillators in both deterministic and stochastic environments can reflect the optimization problem of an organism's circadian clock. Our approach of analyzing the circadian clock can provide us an insight to regulate the operation of a circadian clock within a noisy environment and with internal noise.

Keywords: Biophysics, Circadian Clock, Kuramoto Model, Synchronization, Cost Analysis

Acknowledgements

Firstly, I would like to thank my supervisor Dr. David Sivak for his support and guidance in this research project. Secondly, I would like to thank Dr. Nancy Forde for organizing our final presentation and overseeing this entire two-semesters research course. Last but not the least, I would like to thank the entire Physics Department and my classmates, who had not only taught me valuable knowledge and being supportive throughout my undergraduate career but also helped me to become a critical thinker and a passionate learner.

Table of Contents

List of Figures

Chapter 1

Introduction

The 24-hour sleep-wake cycle is definitely not an exclusively human trait. In fact, this is a common physiological process called the circadian clock (or circadian rhythm) that can be found among mammals, plants and even cyanobacteria.[2][3][4] Moreover, the definition of the circadian clock is far more than just a sleep-wake 24 hour cycle that tracks the solar time. Much research has shown that the circadian clock is linked to our optimal feeding pattern, hormone production, cognitive ability and beyond. Recent research suggested that obesity and metabolic syndrome were observed in mutant mice with no circadian clock gene.[5]

The possession of the clock gene in our DNA is beneficial to us in terms of health and capitalizing on environmental resources. However, there are other so-called free-running organisms that are not entrained to the 24-hour solar time when they are in an environment without external stimulus. Their sleep-wake cycle is out of phase with other circadian clocks in their gene.[6] Therefore, it is not hard to imagine that there are cost-driven optimal responses for a living organism to decide whether they should stay synchronized with the external stimulus such as the sun. In this thesis, we will provide a general framework to interpret the level of optimization of an organism's circadian oscillator by performing cost analysis, based on the phase mismatch between the solar cycle oscillator and an organism's own circadian oscillator.

In fact, there are many mathematical models that biologists currently use to model the mammalian circadian clocks. One type of model relies on the mutual coupling between multiple oscillators, similar to the Kuramoto model.[7] The other type of model relies on computational biological simulations of interactions between different cells and genes. The latter model type has its own disadvantage: computational inconvenience. In order to simulate a biological event, a large numbers of variables need to be introduced within a set of equations to describe all the biological interactions.[8] As a result, they are computationally heavy and overly complicated matters, unlike the one that we are proposing.

Actually, it is quite fascinating that a mammalian circadian clock is synchronized with solar time so naturally. But such a phenomenon is not unique, as there are many similar ex-

amples of stable phase synchronization in nature, like the synchronization of metronomes, birds flying in a group, and flashing of fireflies.[9] These common phenomena of collective synchronization motivated the search for mathematical equations to describe them. The most popular current model that describes these phenomena is called the Kuramoto model.[9] This new mathematical approach was formulated by Winfree based on limit-cycle oscillators with a shared coupling function. Kuramoto expanded upon Winfree's work and solved the model with the perturbation method and equally weighted sinusoidal coupling.[9]

The entrainability of a circadian clock suggests that it can be modeled by the Kuramoto model. In other words, this property of circadian rhythm indicates that an organism's internal clock oscillator can be coupled to an external stimulus such as the sun. The value of the coupling constant is directly proportional to the strength of influence. Another property of a circadian oscillator is a particular organism can have a different preferred frequency of oscillation. One example is the trashline orbweaver, which has a circadian clock of 18.5 hour cycle, but can be entrained to a 24 hour solar cycle. [10] This implies different organisms can have their own circadian oscillator with distinctive intrinsic frequency, but still be coupled to the same solar-cycle oscillator.

Beyond the solar-cycle oscillator, numerous environmental factors can keep the sleep-wake cycle of the organism out of phase with other circadian clocks embedded in other biological constituents. The absence of accurately measured external cues can affect the sleep-wake cycle of organisms. This leads to the use of a stochastic Kuramoto model. Noise in the model can either come from the environment, uncertainty in the internal processing of the organism, or both. An organism can be free-running when their access to the external environment is partially or totally shielded.

To explore the optimal regulation of the circadian clock, we chose the deterministic and stochastic versions of the modified Kuramoto model as equations of motion for an organism's circadian clock. To simplify the problem, we assume an organism just has one circadian clock, even though that is generally not true: there are different circadian clocks within an organism, responsible for the sleep-wake cycle, cell reproduction and brain-wave activities, etc. However, these different circadian clocks have their own internal and external cues of operations, and thus can be treated as totally independent oscillators.

In this thesis, we exclusively focus on the circadian clock that is tracking the solar time cycle. By assuming that the circadian clock oscillator is operating in its most optimal setting when its phase is perfectly in sync with the solar cycle oscillator, we can model that the cost of operating a circadian clock is proportional to the phase mismatch between the two oscillators. In addition, either an organism is within a noisy environment or has noisy internal biological mechanisms, giving the organism a harder time to couple with the other oscillator, hence we expect these conditions will increase the cost of operating the circadian clock. In this thesis, we will explore the behavior of such a system under separate analysis of these various cases.

Chapter 2

Theoretical Background

2.1 Models of Synchronization of Circadian Clocks

The classical Kuramoto model describes frequency synchronization among a network of limit-cycle oscillators.[9] By assuming each individual oscillator i has internal frequency ω_i, and a network of such oscillators are mutually coupled to a nearby oscillator j, the model can be written as:

$$\dot{\theta}_i = \omega_i + \sum_{j=1}^{N} K_{i,j} \sin(\theta_j - \theta_i), \qquad i = 1, ..., N, \qquad K_{i,j} \geqslant 0. \tag{2.1}$$

where θ is the phase of each oscillator, N is the number of oscillators within the network, and $K_{i,j}$ is the mutual coupling constant shared among each pair of coupled oscillators i and j.[9] For a large network of oscillators, the mutual couplings produce a many-body problem, that can be reduced to a single-body problem using the mean-field approximation.[9] Hence, the model of Eq. 2.1 can be rewritten as:

$$\dot{\theta}_i = \omega_i + \frac{K}{N} \sum_{j=1}^{N} \sin(\theta_j - \theta_i), \qquad i = 1, ..., N, \qquad K \geqslant 0. \tag{2.2}$$

We modify the classical Kuramoto model to have a solar-cycle oscillator with dynamics given by:

$$\theta_{\mathrm{s}}(t) = \omega_{\mathrm{s}} \times t, \qquad \dot{\theta}_{\mathrm{s}} = \omega_{\mathrm{s}}, \tag{2.3}$$

where θ_{s} is the phase of the solar-cycle oscillator with natural internal frequency of ω_{s}. The solar cycle oscillator is not entrained by any external source, therefore no coupling is present in the equation. By contrast, the other oscillator in our model (which represents an organism's circadian clock) is coupled to the solar-cycle oscillator according to:

$$\dot{\theta}_{\mathrm{m}} = \omega_{\mathrm{m}} + K \sin(\theta_{\mathrm{s}} - \theta_{\mathrm{m}}), \qquad K \geqslant 0, \tag{2.4}$$

where θ_{m} is the phase of the circadian-clock oscillator of an organism with internal frequency ω_{m} and coupled to the solar-cycle oscillator θ_{s} via external entrainment. The time-courses A_{s} and A_{m} of the level of each oscillator are given by

$$A_{\mathrm{s}} = B_{\mathrm{s}} \sin(\theta_{\mathrm{s}}), \qquad A_{\mathrm{m}} = B_{\mathrm{m}} \sin(\theta_{\mathrm{m}}), \tag{2.5}$$

where B_{s} and B_{m} are the factors scaling A_{s} and A_{m} to appropriate units.

In the real world, there is always random noise that can affect an organism's response to internal and external entrainment. For the case of internal noise, an additive noise is introduced to Eq. 2.2. The stochastic modified Kuramoto model can be rewritten as a Langevin equation if the noise is a Gaussian white noise:

$$\dot{\theta}^{*}_{\mathrm{m,int}} = \omega_{\mathrm{m}} + K \sin(\theta_{\mathrm{s}} - \theta_{\mathrm{m}}) + c_{\mathrm{int}} \xi_{\mathrm{int}}, \tag{2.6}$$

where c_{int} is a scaling factor of the internal noise level, and * in $\dot{\theta}^{*}_{\mathrm{m,int}}$ indicates that the differential equation is stochastic with additive noise ξ_{int} that influences the organism's perception of internal frequency ω_{m}. The additive noise ξ_{int} has zero expectation value:

$$\langle \xi_{\mathrm{int}}(t) \rangle = 0. \tag{2.7}$$

For noise from the external environment, we introduce it inside the sinusoidal coupling function of Eq. 2.2, with the second subscript s in indicating that the noise affects the organism's measurement of external stimulus θ_{s}:

$$\dot{\theta}^{*}_{\mathrm{m,ext}} = \omega_{\mathrm{m}} + K \sin(\theta_{\mathrm{s}} - \theta_{\mathrm{m}} + c_{\mathrm{ext}} \xi_{\mathrm{ext}}), \tag{2.8}$$

where c_{ext} is a scaling factor of the external noise level, and ξ_{ext} is the noise affecting the external entrainment of the circadian oscillator with zero expectation value

$$\langle \xi_{\mathrm{ext}}(t) \rangle = 0. \tag{2.9}$$

It is useful to inspect Eq. 2.8 in more detail since the external noise is embedded inside the coupling function. We can group $c_{\mathrm{ext}} \xi_{\mathrm{ext}}$ together with θ_{s}:

$$\theta^{*}_{\mathrm{s}} = \theta_{\mathrm{s}} + c_{\mathrm{ext}} \xi_{\mathrm{ext}} = \omega_{\mathrm{s}} \times t + c_{\mathrm{ext}} \xi_{\mathrm{ext}} = \omega_{\mathrm{s}} \times (t + \frac{c_{\mathrm{ext}} \xi_{\mathrm{ext}}}{\omega_{\mathrm{s}}}) \tag{2.10}$$

where * indicates that the current θ^{*}_{s} is stochastic. Moreover, after some algebraic manipulations as shown in Eq. 2.10, we can redefine the stochastic version of θ_{s} that has the time-delay property:

$$\tau^{*} = \frac{c_{\mathrm{ext}} \xi_{\mathrm{ext}}}{\omega_{\mathrm{s}}}, \qquad \theta^{*}_{\mathrm{s}} = \omega_{\mathrm{s}} \times (t + \tau^{*}) = \theta_{\mathrm{s}}(t + \tau^{*}), \tag{2.11}$$

where τ^* denotes the time-delay stochastic constant. It is interesting to see that Eq. 2.8 also has time-delay property which can be overlooked at first. By combining Eq. 2.10 and 2.11, we can rewrite Eq. 2.8 as:

$$\dot{\theta}^*_{\mathrm{m,ext}} = \omega_{\mathrm{m}} + K\sin(\theta_{\mathrm{s}}(t+\tau^*) - \theta_{\mathrm{m}}). \tag{2.12}$$

This is difficult to solve, since the noise can turn out to be a multiplicative noise, and the time-delayed Kuramoto model is relatively unexplored. The stochastic version of our modified Kuramoto model with both external and internal noise can be written as:

$$\dot{\theta}^{**}_{\mathrm{m}} = \omega_{\mathrm{m}} + K\sin(\theta_{\mathrm{s}} - \theta_{\mathrm{m}} + c_{\mathrm{ext}}\xi_{\mathrm{ext}}) + c_{\mathrm{int}}\xi_{\mathrm{int}} \tag{2.13a}$$

$$\dot{\theta}^{**}_{\mathrm{m}} = \omega_{\mathrm{m}} + K\sin(\theta_{\mathrm{s}}(t+\tau^*) - \theta_{\mathrm{m}}) + c_{\mathrm{int}}\xi_{\mathrm{int}} \tag{2.13b}$$

where ** in $\dot{\theta}^{**}_{\mathrm{m}}$ indicates that the equation of motion includes two stochastic processes.

2.2 Methods of ODE and SDE Integrations

The most common numerical integration methods for the Kuramoto model is the fourth-order Runge-Kutta method for the deterministic case, and the Euler-Maruyama method for the stochastic case.[11] [12] However, these two commonly used methods are not time-reversible, hence we develop our own integration methods. The deterministic and stochastic version of our modified Kuramoto model can be numerically integrated by the time-reversible deterministic and stochastic leapfrog integrator.

2.2.1 Deterministic Leapfrog Integrator

For our deterministic model, one iteration of numerical integration can be split into two fractional steps, with each fractional step updating θ_{m} over half of a full time step. Such integration method is discussed in Sivak et. al.'s "Time Step Rescaling Recovers Continuous-Time Dynamical Properties for Discrete-Time Langevin Integration of Nonequilibrium Systems".[13] Following their integration method, we develop a new integration algorithm for our modified Kuramoto model:

$$\theta_{\mathrm{m,n+\frac{1}{2}}} = \theta_{\mathrm{m,n}} + \frac{1}{2}\frac{d\theta_{\mathrm{m,n}}}{dt}\Delta t \tag{2.14a}$$

$$= \theta_{\mathrm{m,n}} + \frac{1}{2}[\omega_{\mathrm{m}} + K\sin(\theta_{\mathrm{s,n}} - \theta_{\mathrm{m,n}})]\Delta t, \tag{2.14b}$$

$$\theta_{\mathrm{m,n+1}} = \theta_{\mathrm{m,n+\frac{1}{2}}} + \frac{1}{2}\frac{d\theta_{\mathrm{m,n+\frac{1}{2}}}}{dt}\Delta t \tag{2.14c}$$

$$= \theta_{\mathrm{m,n+\frac{1}{2}}} + \frac{1}{2}[\omega_{\mathrm{m}} + K\sin(\theta_{\mathrm{s,n+\frac{1}{2}}} - \theta_{\mathrm{m,n+\frac{1}{2}}})]\Delta t \tag{2.14d}$$

where Δt is the step-size in time and n denotes the current step.

2.2.2 Stochastic Leapfrog Integrator - Wiener Process

For the stochastic version of our modified Kuramoto model, we have to define the stochastic process used in our modeling. The Wiener process is the most commonly applied stochastic process in modeling of the stochastic Kuramoto model. [12] However, it is mathematically challenging to solve its probability density function. Instead, we primarily use a differentiable Gaussian process in our analysis. But we can still construct our numerical integration method using a Wiener process, because it is a topic that may reward further study.

By definition, each increment of a Wiener process is independent and has a normal distribution, $\mathcal{N}(0, \Delta t)$. The Wiener process can be defined by:

$$W_{\mathrm{t}+\Delta\mathrm{t}} - W_{\mathrm{t}} = \Delta W_{\mathrm{t}} \sim \mathcal{N}(0, \Delta t) \ , \tag{2.15}$$

where W_t is the Wiener process at time t and ΔW_t is an independent increment of the Wiener process. A Gaussian white noise ξ_{int} in Eq. 2.6 can be replaced as an increment of the Wiener process:

$$\Delta W_{\mathrm{t}} \sim \mathcal{N}(0, \Delta t) = \xi_{\mathrm{int}}(t), \qquad \sigma^2_{\mathrm{int}} = \langle \delta\xi^2_{\mathrm{int}}(t) \rangle = \Delta t. \tag{2.16}$$

Then the leapfrog integrator of Eq. 2.14 needs to take the new stochastic component into consideration. From the above mentioned paper: "Time Step Rescaling Recovers Continuous-Time Dynamical Properties for Discrete-Time Langevin Integration of Nonequilibrium Systems", the stochastic leapfrog integrator can be implemented with the stochastic and deterministic component integrated separately.[13] Hence, we develop a new stochastic leapfrog integrator for our model, according to the algorithm:

$$\theta_{\mathrm{m,n}+\frac{1}{4}} = \theta_{\mathrm{m,n}} + \frac{1}{2} c \Delta W_{\mathrm{n}}, \tag{2.17a}$$

$$\theta_{\mathrm{m,n}+\frac{1}{2}} = \theta_{\mathrm{m,n}+\frac{1}{4}} + \frac{1}{2} \frac{d\theta_{\mathrm{m,n}+\frac{1}{4}}}{dt} \Delta t \tag{2.17b}$$

$$= \theta_{\mathrm{m,n}+\frac{1}{4}} + \frac{1}{2} [\omega_{\mathrm{m}} + K \sin(\theta_{\mathrm{s,n}+\frac{1}{4}} - \theta_{\mathrm{m,n}+\frac{1}{4}})] \Delta t, \tag{2.17c}$$

$$\theta_{\mathrm{m,n}+\frac{3}{4}} = \theta_{\mathrm{m,n}+\frac{1}{2}} + \frac{1}{2} \frac{d\theta_{\mathrm{m,n}+\frac{1}{2}}}{dt} \Delta t \tag{2.17d}$$

$$= \theta_{\mathrm{m,n}+\frac{1}{2}} + \frac{1}{2} [\omega_{\mathrm{m}} + K \sin(\theta_{\mathrm{s,n}+\frac{1}{2}} - \theta_{\mathrm{m,n}+\frac{1}{2}})] \Delta t, \tag{2.17e}$$

$$\theta_{\mathrm{m,n+1}} = \theta_{\mathrm{m,n}+\frac{3}{4}} + \frac{1}{2} c \Delta W_{\mathrm{n+1}}. \tag{2.17f}$$

The same stochastic process can be used to model the other Gaussian white noise we introduced in Eq. 2.8, the noise ξ_{ext} from the external environment:

$$\Delta W_{\mathrm{t}} \sim \mathcal{N}(0, \Delta t) = \xi_{\mathrm{ext}}(t), \qquad \sigma^2_{\mathrm{ext}} = \langle \delta\xi^2_{\mathrm{ext}}(t) \rangle = \Delta t. \tag{2.18}$$

Similar to Eq. 2.17, the stochastic leapfrog integrator for the SDE with Gaussian white noise within the sinusoidal coupling function can be implemented as:

$$\theta^{*}_{\mathrm{s,n}} = \theta_{\mathrm{s,n}} + \frac{1}{2} b \Delta W_{\mathrm{n}}, \tag{2.19a}$$

$$\theta_{\mathrm{m,n+\frac{1}{2}}} = \theta_{\mathrm{m,n}} + \frac{1}{2} \frac{d\theta_{\mathrm{m,n}}}{dt} \Delta t \tag{2.19b}$$

$$= \theta_{\mathrm{m,n}} + \frac{1}{2} [\omega_{\mathrm{m}} + K \sin(\theta^{*}_{\mathrm{s,n}} - \theta_{\mathrm{m,n}})] \Delta t, \tag{2.19c}$$

$$\theta^{*}_{\mathrm{s,n+\frac{1}{2}}} = \theta_{\mathrm{s,n+\frac{1}{2}}} + \frac{1}{2} b \Delta W_{\mathrm{n+1}}, \tag{2.19d}$$

$$\theta_{\mathrm{m,n+1}} = \theta_{\mathrm{m,n+\frac{1}{2}}} + \frac{1}{2} \frac{d\theta_{\mathrm{m,n+\frac{1}{2}}}}{dt} \Delta t \tag{2.19e}$$

$$= \theta_{\mathrm{m,n+\frac{1}{2}}} + \frac{1}{2} [\omega_{\mathrm{m}} + K \sin(\theta^{*}_{\mathrm{s,n+\frac{1}{2}}} - \theta_{\mathrm{m,n+\frac{1}{2}}})] \Delta t, \tag{2.19f}$$

Note that the integration step of the stochastic component in Eq. 2.19 is different compare to Eq. 2.17 because the external noise ξ_{ext} affects the value of θ_{s} inside the sinusoidal function for each fractional step of integration. By combining Eq. 2.17 and 2.19, we develop a stochastic leapfrog integrator for Eq. 2.13:

$$\theta_{\mathrm{m,n+\frac{1}{4}}} = \theta_{\mathrm{m,n}} + \frac{1}{2} c \Delta W_{\mathrm{m,n}}, \tag{2.20a}$$

$$\theta^{*}_{\mathrm{s,n+\frac{1}{4}}} = \theta_{\mathrm{s,n+\frac{1}{4}}} + \frac{1}{2} b \Delta W_{\mathrm{s,n}}, \tag{2.20b}$$

$$\theta_{\mathrm{m,n+\frac{1}{2}}} = \theta_{\mathrm{m,n+\frac{1}{4}}} + \frac{1}{2} \frac{d\theta_{\mathrm{m,n+\frac{1}{4}}}}{dt} \Delta t \tag{2.20c}$$

$$= \theta_{\mathrm{m,n+\frac{1}{4}}} + \frac{1}{2} [\omega_{\mathrm{m}} + K \sin(\theta^{*}_{\mathrm{s,n+\frac{1}{4}}} - \theta_{\mathrm{m,n+\frac{1}{4}}})] \Delta t, \tag{2.20d}$$

$$\theta^{*}_{\mathrm{s,n+\frac{1}{2}}} = \theta_{\mathrm{s,n+\frac{1}{2}}} + \frac{1}{2} b \Delta W_{\mathrm{s,n+1}}, \tag{2.20e}$$

$$\theta_{\mathrm{m,n+\frac{3}{4}}} = \theta_{\mathrm{m,n+\frac{1}{2}}} + \frac{1}{2} \frac{d\theta_{\mathrm{m,n+\frac{1}{2}}}}{dt} \Delta t \tag{2.20f}$$

$$= \theta_{\mathrm{m,n+\frac{1}{2}}} + \frac{1}{2} [\omega_{\mathrm{m}} + K \sin(\theta^{*}_{\mathrm{s,n+\frac{1}{2}}} - \theta_{\mathrm{m,n+\frac{1}{2}}})] \Delta t, \tag{2.20g}$$

$$\theta_{\mathrm{m,n+1}} = \theta_{\mathrm{m,n+\frac{3}{4}}} + \frac{1}{2} c \Delta W_{\mathrm{m,n+1}}. \tag{2.20h}$$

In the next section, we will begin to explore the stochastic Kuramoto model under the noise driven by a differentiable Gaussian process.

2.2.3 Stochastic Differential Equation Integrator - Gaussian Process

To define a differentiable Gaussian process [14], we first predefine a normal distribution of a set of random variables from time $0 \longrightarrow t$ as:

$$G(0) = 0, \qquad G(t) \sim \mathcal{N}(0, \Delta t), \tag{2.21}$$

where G represents the Gaussian process, with normal distribution $\mathcal{N}(0, \Delta t)$.[14] An increment ΔG_t of the Gaussian process is the difference between subsequent random variables in time $G_{t+\Delta t} - G_t$, such that

$$\Delta G_t = G_{t+\Delta t} - G_t, \qquad \mathbf{Cov}[\Delta G_t, \Delta G_{t+\Delta t}] = -|\Delta t|, \tag{2.22}$$

where **Cov** is the covariance of a random dataset. The noise in Eq. 2.6 can be implemented as an increment of the Gaussian process in the same way as the Wiener process in Eq. 2.15:

$$\Delta G_t = \xi_{\text{int}}(t), \qquad \mathbf{Cov}[\xi_{\text{int}}(t), \xi_{\text{int}}(t + \Delta t)] = -|\Delta t|. \tag{2.23}$$

The stochastic leapfrog integrator in this case is still similar to Eq. 2.17, but the Wiener process W is replaced with the Gaussian process G, giving the new algorithm

$$\theta_{\text{m,n}+\frac{1}{4}} = \theta_{\text{m,n}} + \frac{1}{2} c \Delta G_{\text{n}}, \tag{2.24a}$$

$$\theta_{\text{m,n}+\frac{1}{2}} = \theta_{\text{m,n}+\frac{1}{4}} + \frac{1}{2} \frac{d\theta_{\text{m,n}+\frac{1}{4}}}{dt} \Delta t \tag{2.24b}$$

$$= \theta_{\text{m,n}+\frac{1}{4}} + \frac{1}{2} [\omega_{\text{m}} + K \sin(\theta_{\text{s,n}+\frac{1}{4}} - \theta_{\text{m,n}+\frac{1}{4}})] \Delta t, \tag{2.24c}$$

$$\theta_{\text{m,n}+\frac{3}{4}} = \theta_{\text{m,n}+\frac{1}{2}} + \frac{1}{2} \frac{d\theta_{\text{m,n}+\frac{1}{2}}}{dt} \Delta t \tag{2.24d}$$

$$= \theta_{\text{m,n}+\frac{1}{2}} + \frac{1}{2} [\omega_{\text{m}} + K \sin(\theta_{\text{s,n}+\frac{1}{2}} - \theta_{\text{m,n}+\frac{1}{2}})] \Delta t, \tag{2.24e}$$

$$\theta_{\text{m,n}+1} = \theta_{\text{m,n}+\frac{3}{4}} + \frac{1}{2} c \Delta G_{\text{n}+1}. \tag{2.24f}$$

Also Eq. 2.19 can be rewritten as:

$$\theta^*_{\text{s,n}+\frac{1}{4}} = \theta_{\text{s,n}+\frac{1}{4}} + \frac{1}{2} b \Delta G_{\text{s,n}}, \tag{2.25a}$$

$$\theta_{\text{m,n}+\frac{1}{2}} = \theta_{\text{m,n}+\frac{1}{4}} + \frac{1}{2} \frac{d\theta_{\text{m,n}+\frac{1}{4}}}{dt} \Delta t \tag{2.25b}$$

$$= \theta_{\text{m,n}+\frac{1}{4}} + \frac{1}{2} [\omega_{\text{m}} + K \sin(\theta^*_{\text{s,n}+\frac{1}{4}} - \theta_{\text{m,n}+\frac{1}{4}})] \Delta t, \tag{2.25c}$$

$$\theta^*_{\text{s,n}+\frac{1}{2}} = \theta_{\text{s,n}+\frac{1}{2}} + \frac{1}{2} b \Delta G_{\text{s,n}+1}, \tag{2.25d}$$

$$\theta_{\text{m,n}+\frac{3}{4}} = \theta_{\text{m,n}+\frac{1}{2}} + \frac{1}{2} \frac{d\theta_{\text{m,n}+\frac{1}{2}}}{dt} \Delta t \tag{2.25e}$$

$$= \theta_{\text{m,n}+\frac{1}{2}} + \frac{1}{2} [\omega_{\text{m}} + K \sin(\theta^*_{\text{s,n}+\frac{1}{2}} - \theta_{\text{m,n}+\frac{1}{2}})] \Delta t. \tag{2.25f}$$

Finally, the complete algorithm of Eq. 2.20 becomes:

$$\theta_{\mathrm{m,n+\frac{1}{4}}} = \theta_{\mathrm{m,n}} + \frac{1}{2}c\Delta G_{\mathrm{m,n}}, \tag{2.26a}$$

$$\theta^{*}_{\mathrm{s,n+\frac{1}{4}}} = \theta_{\mathrm{s,n+\frac{1}{4}}} + \frac{1}{2}b\Delta G_{\mathrm{s,n}}, \tag{2.26b}$$

$$\theta_{\mathrm{m,n+\frac{1}{2}}} = \theta_{\mathrm{m,n+\frac{1}{4}}} + \frac{1}{2}\frac{d\theta_{\mathrm{m,n+\frac{1}{4}}}}{dt}\Delta t \tag{2.26c}$$

$$= \theta_{\mathrm{m,n+\frac{1}{4}}} + \frac{1}{2}[\omega_{\mathrm{m}} + K\sin(\theta^{*}_{\mathrm{s,n+\frac{1}{4}}} - \theta_{\mathrm{m,n+\frac{1}{4}}})]\Delta t, \tag{2.26d}$$

$$\theta^{*}_{\mathrm{s,n+\frac{1}{2}}} = \theta_{\mathrm{s,n+\frac{1}{2}}} + \frac{1}{2}b\Delta G_{\mathrm{s,n+1}}, \tag{2.26e}$$

$$\theta_{\mathrm{m,n+\frac{3}{4}}} = \theta_{\mathrm{m,n+\frac{1}{2}}} + \frac{1}{2}\frac{d\theta_{\mathrm{m,n+\frac{1}{2}}}}{dt}\Delta t \tag{2.26f}$$

$$= \theta_{\mathrm{m,n+\frac{1}{2}}} + \frac{1}{2}[\omega_{\mathrm{m}} + K\sin(\theta^{*}_{\mathrm{s,n+\frac{1}{2}}} - \theta_{\mathrm{m,n+\frac{1}{2}}})]\Delta t, \tag{2.26g}$$

$$\theta_{\mathrm{m,n+1}} = \theta_{\mathrm{m,n+\frac{3}{4}}} + \frac{1}{2}c\Delta G_{\mathrm{m,n+1}}. \tag{2.26h}$$

2.3 Critical Coupling

The frequency of a circadian clock oscillator $\dot{\theta_{\mathrm{m}}}$ is expected to be synchronized with the solar-cycle frequency ω_{s} if the coupling constant K between oscillators is above a threshold value, known as the critical coupling constant K_c.

2.3.1 Deterministic Model

For the deterministic version of our modified Kuramoto model Eq. 2.4, a circadian oscillator is synchronized with the solar cycle oscillator when:

$$\omega_{\mathrm{s}} = \omega_{\mathrm{m}} + K\sin(\theta_{\mathrm{s}} - \theta_{\mathrm{m}}), \qquad K \geq K_{\mathrm{c}}. \tag{2.27}$$

The critical coupling constant K_{c} is the smallest value of K which can achieve the above steady state condition Eq. 2.27. We minimize K_{c} in Eq. 2.27 by maximizing the sinusoidal coupling function,

$$\sin(\theta_{\mathrm{s}} - \theta_{\mathrm{m}}) = 1, \qquad \theta_{\mathrm{s}} - \theta_{\mathrm{m}} = \frac{\pi}{2}. \tag{2.28}$$

Substituting Eq.2.28 into 2.27, we obtain:

$$|\omega_{\mathrm{s}} - \omega_{\mathrm{m}}| = K_{\mathrm{c}}, \qquad \Delta\omega = \omega_{\mathrm{s}} - \omega_{\mathrm{m}}, \qquad K_{\mathrm{c}} = |\Delta\omega|, \tag{2.29}$$

where the absolute value of $\Delta\omega$ emphasizes the coupling constant K is always positive as define in Eq.2.4.

2.3.2 Stochastic Model with Wiener Process

For any stochastic differential equation in the form of:

$$d\theta_t = \mu(\theta_t, t)dt + \sigma(\theta_t, t)dW_t, \tag{2.30}$$

where dW_t is an increment of the Wiener process, one can always write the Fokker-Planck equation [15] with probability density function $\rho(\theta, t)$ of the random variables θ as follow:

$$\frac{\partial}{\partial t}\rho(\theta, t) = -\frac{\partial}{\partial \theta}[\mu(\theta, t)\rho(\theta, t)] + \frac{\partial^2}{\partial \theta^2}[D(\theta, t)\rho(\theta, t)], \tag{2.31}$$

where the diffusion coefficient $D(\theta, t) = \sigma^2(\theta_t, t)/2$.[15] In our case, it is not difficult to realize that Eq.2.6 is precisely in the form of Eq.2.30, so we substitute Eq.2.6 into 2.31, giving

$$\frac{\partial}{\partial t}\rho(\theta_{\mathrm{m}}, t) = -\frac{\partial}{\partial \theta_{\mathrm{m}}}[(\omega_{\mathrm{m}} + K\sin(\theta_{\mathrm{s}} - \theta_{\mathrm{m}}))\rho(\theta_{\mathrm{m}}, t)] + \frac{\partial^2}{\partial \theta_{\mathrm{m}}^2}[D\rho(\theta_{\mathrm{m}}, t)], \tag{2.32}$$

where $D = c_{\mathrm{int}}^2 \Delta t/2$ define by Eq. 2.15 and 2.6.[9] After some simplifications, we can rewrite the above partial differential equation as:

$$\frac{\partial \rho}{\partial t} = K\cos(\theta_{\mathrm{s}} - \theta_{\mathrm{m}})\rho - [\omega_{\mathrm{m}} + K\sin(\theta_{\mathrm{s}} - \theta_{\mathrm{m}})]\frac{\partial \rho}{\partial \theta_{\mathrm{m}}} + D\frac{\partial^2 \rho}{\partial \theta_{\mathrm{m}}^2}. \tag{2.33}$$

To obtain the critical coupling constant K_{c} for the stochastic Kuramoto model with the Wiener process, we have to solve $\rho(\theta_{\mathrm{m}}, t)$ from the above Fokker Planck equation Eq. 2.33. However, the exact analytic form of $\rho(\theta_{\mathrm{m}}, t)$ is yet to be found. The current approach to analyze such stochastic model is by using Fourier series to approximate $\rho(\theta_{\mathrm{m}}, t)$ and the mathematics involved in deriving K_c with approximated form of $\rho(\theta_{\mathrm{m}}, t)$ is still under active investigation by mathematicians and physicists.[9] It is beyond the scope of this thesis to solve K_{c} from the stochastic model with the Wiener process. But this is not the case when we define the stochastic process in our modified model by a differentiable Gaussian process, since we have previously defined the probability distribution of the random variables in Eq. 2.21, therefore we can calculate the expected value of the differential equation at steady state to derive K_c.

2.3.3 Stochastic Model with Gaussian Process (Internal Noise)

A circadian clock can synchronize with the solar-cycle oscillator even when there is internal noise inside the organism. We can rewrite Eq. 2.6 with the assumption that above statement Eq. 2.27 holds, with $K \geq K^*_{\mathrm{c,int}}$:

$$\omega_{\mathrm{s}} = \omega_{\mathrm{m}} + K^*_{\mathrm{c,int}}\sin(\theta_{\mathrm{s}} - \theta_{\mathrm{m}}) + c_{\mathrm{int}}\xi_{\mathrm{int}}, \quad \Delta\omega = K^*_{\mathrm{c,int}}\sin(\theta_{\mathrm{s}} - \theta_{\mathrm{m}}) + c_{\mathrm{int}}\xi_{\mathrm{int}}, \tag{2.34}$$

where $K^*_{\mathrm{c,int}}$ is the critical coupling constant for the case of an organism experiencing internal noise. As discussed in the previous section, the benefit of working with the Gaussian process is that the distribution of the random variable is known, and we can get the expected value of Eq. 2.34 to derive the equation for $K^*_{\mathrm{c,int}}$. In other words, we can always calculate Eq. 2.6 in terms of the Itô integral:

$$\int_{\theta(0)}^{\theta(t)} d\theta = \int_0^t [\omega_{\mathrm{m}} + K\sin(\theta_{\mathrm{s}} - \theta_{\mathrm{m}})]dt + c_{\mathrm{int}} \int_0^t dG_t \tag{2.35a}$$

$$\theta_{\mathrm{m}}(t) = \theta_{\mathrm{m}}(0) + \int_0^t [\omega_{\mathrm{m}} + K\sin(\theta_{\mathrm{s}} - \theta_{\mathrm{m}})]dt + c_{\mathrm{int}}[G(t) - G(0)] \tag{2.35b}$$

$$\theta_{\mathrm{m}}(t) = \theta_{\mathrm{m}}(0) + \int_0^t [\omega_{\mathrm{m}} + K\sin(\theta_{\mathrm{s}} - \theta_{\mathrm{m}})]dt + c_{\mathrm{int}}G(t), \tag{2.35c}$$

where we know precisely how $G(t)$ affects θ_{m}. For this reason, we take the expectation value of Eq. 2.34 in this way:

$$\mathbf{E}[\Delta\omega] = \mathbf{E}[K^*_{\mathrm{c,int}}\sin(\theta_{\mathrm{s}} - \theta_{\mathrm{m}})] + \mathbf{E}[c_{\mathrm{int}}\xi_{\mathrm{int}}], \quad \langle\xi_{\mathrm{int}}(t)\rangle = 0, \quad \mathbf{E}[c_{\mathrm{int}}\xi_{\mathrm{int}}] = 0, \tag{2.36}$$

where $\mathbf{E}$ denotes the expectation value. We can simplify the above operation by noting that $\Delta\omega$ is a constant:

$$\mathbf{E}[\Delta\omega] = \Delta\omega, \quad \Delta\omega = K^*_{\mathrm{c,int}}\mathbf{E}[\sin(\theta_{\mathrm{s}} - \theta^*_{\mathrm{m}})], \tag{2.37}$$

where * indicates that the variable is stochastic. Therefore by applying the definition of expected value, we are left with:

$$\mathbf{E}[\sin(\theta_{\mathrm{s}} - \theta^*_{\mathrm{m}})] = \int_{-\infty}^{\infty} d\theta^*_{\mathrm{m}} P(\theta^*_{\mathrm{m}})\sin(\theta_{\mathrm{s}} - \theta^*_{\mathrm{m}}), \tag{2.38}$$

where $P(\theta^*_{\mathrm{m}})$ is the normal distribution that we defined for the Gaussian process for random variables θ^*_{m}. And c_{int} in Eq. 2.6 scales the standard deviation of the normally distributed random variable θ^*_{m}, and θ^*_{m} has standard deviation of $\sqrt{\Delta t}$, as given by Eq. 2.21. The mean value of θ^*_{m} can be obtained from the deterministic case where $\theta_{\mathrm{s}} - \theta_{\mathrm{m}} = \frac{\pi}{2}$, and then $P(\theta^*_{\mathrm{m}})$ is a normal distribution given by:

$$P(\theta^*_{\mathrm{m}}) = \frac{1}{\sqrt{2\pi(c_{\mathrm{int}}\sigma_{\mathrm{int}})^2}} \exp\left[\frac{-(\theta^*_{\mathrm{m}} - \theta_{\mathrm{s}} + \frac{\pi}{2})^2}{2(c_{\mathrm{int}}\sigma_{\mathrm{int}})^2}\right], \qquad \sigma_{\mathrm{int}} = \sqrt{\Delta t}, \tag{2.39}$$

We change variables, setting $s = [2(c_{\mathrm{int}}\sigma_{\mathrm{int}})^2]^{-1}$ and $x = \theta^*_{\mathrm{m}} - \theta_{\mathrm{s}} + \frac{\pi}{2}$ which Eq. 2.39 becomes:

$$P(x) = \sqrt{\frac{s}{\pi}}\exp[-sx^2], \tag{2.40}$$

then, we substitute the above equation back to the integral, so that Eq. 2.38 becomes:

$$\mathbf{E}[\sin(\theta_{\mathrm{s}} - \theta_{\mathrm{m}}^*)] = \int_{-\infty}^{\infty} dx P(x) \sin\left(\frac{\pi}{2} - x\right) \tag{2.41a}$$

$$= \int_{-\infty}^{\infty} dx \sqrt{\frac{s}{\pi}} \exp[-sx^2] \sin\left(\frac{\pi}{2} - x\right) \ . \tag{2.41b}$$

Using the trigonometric identity,

$$\sin\left(\frac{\pi}{2} - x\right) = \sin\left(\frac{\pi}{2}\right)\cos(x) - \sin(x)\cos\left(\frac{\pi}{2}\right) = \cos(x), \tag{2.42}$$

simplifies the integral to:

$$\mathbf{E}[\sin(\theta_{\mathrm{s}} - \theta_{\mathrm{m}}^*)] = \int_{-\infty}^{\infty} dx \sqrt{\frac{s}{\pi}} \exp[-sx^2] \cos(x), \tag{2.43a}$$

$$= \frac{1}{2}\Big[\int_{-\infty}^{\infty} dx \sqrt{\frac{s}{\pi}} \exp[-sx^2 + ix] + \int_{-\infty}^{\infty} dx \sqrt{\frac{s}{\pi}} \exp[-sx^2 - ix]\Big] \tag{2.43b}$$

$$= \frac{1}{2}[f(x) + g(x)], \tag{2.43c}$$

$$f(x) = \int_{-\infty}^{\infty} dx \sqrt{\frac{s}{\pi}} \exp[-sx^2 + ix], \qquad g(x) = \int_{-\infty}^{\infty} dx \sqrt{\frac{s}{\pi}} \exp[-sx^2 - ix], \tag{2.44}$$

The equations of Eq. 2.44 are in the form of Fourier transforms, with general solution:

$$\int_{-\infty}^{\infty} dx \exp\left[-\frac{1}{2}ax^2 + iJx\right] = \sqrt{\frac{2\pi}{a}} \exp\left[-\frac{J^2}{2a}\right], \tag{2.45}$$

Therefore, the solutions of $f(x)$ and $g(x)$ are:

$$f(x) = \exp\left[-\frac{1}{4s}\right], \qquad g(x) = \exp\left[-\frac{1}{4s}\right]. \tag{2.46}$$

Finally, substituting Eq. 2.46 into 2.43 gives

$$\mathbf{E}[\sin(\theta_{\mathrm{s}} - \theta_{\mathrm{m}}^*)] = \exp\left[-\frac{1}{4s}\right] \tag{2.47a}$$

$$= \exp\left[\frac{-(c_{\mathrm{int}}\sigma_{\mathrm{int}})^2}{2}\right]. \tag{2.47b}$$

After substituting Eq. 2.47 into 2.37, the expression of the critical coupling constant $K_{\mathrm{c,int}}^*$, reflecting the change in K_c for the stochastic case, is proportional to the standard deviation of the noise σ_{int} and the scaling factor c_{int}:

$$|\Delta\omega| = K_{\mathrm{c,int}}^* \exp\left[\frac{-(c_{\mathrm{int}}\sigma_{\mathrm{int}})^2}{2}\right], \qquad K_{\mathrm{c,int}}^* = |\Delta\omega| \exp\left[\frac{(c_{\mathrm{int}}\sigma_{\mathrm{int}})^2}{2}\right]. \tag{2.48}$$

2.3.4 Stochastic Model with Gaussian Process (External Noise)

As previously discussed, the stochastic Kuramoto model with noise inside the sinusoidal coupling function of Eq. 2.8 is in fact a time-delay stochastic differential equation and it can be challenging to solve. For our modified Kuramoto model with external noise, we can still assume that the circadian clock can be synchronized with the solar cycle oscillator if Eq. 2.8 reaches the following steady state:

$$\omega_{\mathrm{s}} = \omega_{\mathrm{m}} + K\sin(\theta_{\mathrm{s}} - \theta_{\mathrm{m}} + c_{\mathrm{ext}}\xi_{\mathrm{ext}}), \qquad K \geq K^{*}_{\mathrm{c,ext}} \tag{2.49}$$

where $K^{*}_{\mathrm{c,ext}}$ is the critical coupling constant when an organism experiences external noise. We can apply the same analysis from the previous subsection to Eq.2.49, namely taking the expectation value of Eq. 2.49:

$$\mathbf{E}[\Delta\omega] = \mathbf{E}[K^{*}_{\mathrm{c,ext}}\sin(\theta_{\mathrm{s}} - \theta_{\mathrm{m}} + c_{\mathrm{ext}}\xi_{\mathrm{ext}})], \tag{2.50}$$

with knowing that $\Delta\omega$ is a constant, the above equation can be written as:

$$\mathbf{E}[\Delta\omega] = \Delta\omega, \quad \Delta\omega = K^{*}_{\mathrm{c,ext}}\mathbf{E}[\sin(\theta_{\mathrm{s}} - \theta_{\mathrm{m}} + c_{\mathrm{ext}}\xi_{\mathrm{ext}})]\ . \tag{2.51}$$

Using the trigonometric identity

$$\sin\left(\theta_{\mathrm{s}} - \theta_{\mathrm{m}} + c_{\mathrm{ext}}\xi_{\mathrm{ext}}\right) = \sin\left(\theta_{\mathrm{s}} - \theta_{\mathrm{m}}\right)\cos(c_{\mathrm{ext}}\xi_{\mathrm{ext}}) + \cos\left(\theta_{\mathrm{s}} - \theta_{\mathrm{m}}\right)\sin(c_{\mathrm{ext}}\xi_{\mathrm{ext}}), \tag{2.52}$$

and applying the definition of expected value, the integral form of Eq.2.49 reduces to

$$\mathbf{E}[\sin(\theta_{\mathrm{s}} - \theta_{\mathrm{m}} + c_{\mathrm{ext}}\xi_{\mathrm{ext}})] = \sin(\theta_{\mathrm{s}} - \theta_{\mathrm{m}})\int_{-\infty}^{\infty} d\xi_{\mathrm{ext}}P(\xi_{\mathrm{ext}})\cos(c_{\mathrm{ext}}\xi_{\mathrm{ext}}) \tag{2.53a}$$

$$+\cos(\theta_{\mathrm{s}} - \theta_{\mathrm{m}})\int_{-\infty}^{\infty} d\xi_{\mathrm{ext}}P(\xi_{\mathrm{ext}})\sin(c_{\mathrm{ext}}\xi_{\mathrm{ext}}). \tag{2.53b}$$

Note that the prior distribution $P(\xi_{\mathrm{ext}})$ is an even Gaussian function with $\langle\xi_{\mathrm{ext}}(t)\rangle = 0$, whereas $\sin(c_{\mathrm{ext}}\xi_{\mathrm{ext}})$ is an odd function, hence their integral from $-\infty$ to ∞ is zero:

$$\int_{-\infty}^{\infty} d\xi_{\mathrm{ext}}P(\xi_{\mathrm{ext}})\sin(c_{\mathrm{ext}}\xi_{\mathrm{ext}}) = 0. \tag{2.54}$$

The predefined distribution of ξ_{ext} is

$$P(\xi_{\mathrm{ext}}) = \frac{1}{\sqrt{2\pi\sigma^{2}_{\mathrm{ext}}}}\exp\left[\frac{-(\xi_{\mathrm{ext}})^{2}}{2\sigma^{2}_{\mathrm{ext}}}\right], \qquad \sigma_{\mathrm{ext}} = \sqrt{\Delta t}\ . \tag{2.55}$$

Changing variables via $y = \xi_{\text{ext}}$ and $u = [2\sigma_{\text{ext}}^2]^{-1}$, simplifies Eq. 2.55 to:

$$P(y) = \sqrt{\frac{u}{\pi}} \exp[-uy^2], \tag{2.56}$$

and the integral of Eq. 2.53 becomes:

$$\mathbf{E}[\sin(\theta_{\text{s}} - \theta_{\text{m}} + c_{\text{ext}}\xi_{\text{ext}})] = \sin(\theta_{\text{s}} - \theta_{\text{m}})\, b \int_{-\infty}^{\infty} dy P(y) \cos(y) \tag{2.57a}$$

$$= \sin(\theta_{\text{s}} - \theta_{\text{m}})\, b \int_{-\infty}^{\infty} dy \sqrt{\frac{u}{\pi}} \exp[-uy^2] \cos(y). \tag{2.57b}$$

The integral on the right hand side of Eq. 2.57 is in the same form as Eq. 2.43, so that it evaluates to

$$\mathbf{E}[\sin(\theta_{\text{s}} - \theta_{\text{m}} + c_{\text{ext}}\xi_{\text{ext}})] = c_{\text{ext}} \exp\left[-\frac{(c_{\text{ext}}\sigma_{\text{ext}})^2}{2} \right]. \tag{2.58}$$

Substituting Eq. 2.58 into 2.49 gives an expression for $K^*_{\text{c,ext}}$:

$$K^*_{\text{c,ext}} = \frac{|\Delta\omega|}{c_{\text{ext}}} \exp\left[\frac{(c_{\text{ext}}\sigma_{\text{ext}})^2}{2} \right]. \tag{2.59}$$

In contrast to Eq. 2.48, $K^*_{\text{c,ext}}$ is also inversely proportional to the scaling factor c_{ext}.

2.3.5 Stochastic Model with Gaussian Process (Internal and External Noise)

We now follow the same analysis from the previous subsections, so that circadian oscillator in Eq. 2.13 is critically coupled to the solar-cycle oscillator when

$$\omega_{\text{s}} = \omega_{\text{m}} + K \sin(\theta_{\text{s}} - \theta_{\text{m}} + c_{\text{ext}}\xi_{\text{ext}}) + c_{\text{int}}\xi_{\text{int}}, \qquad K \geq K_c^{**}. \tag{2.60}$$

Here K_c^{**} is the critical coupling constant of the system with both external and internal noise. We take the expectation value of Eq. 2.60:

$$\mathbf{E}[\Delta\omega] = K_c^{**}\, \mathbf{E}[\sin(\theta_{\text{s}} - \theta_{\text{m}} + c_{\text{ext}}\xi_{\text{ext}})] + \mathbf{E}[c_{\text{int}}\xi_{\text{int}}]. \tag{2.61}$$

We know that $\mathbf{E}[c_{\text{int}}\xi_{\text{int}}] = 0$ from Eq. 2.36. To show that θ_{m} is randomly distributed, we change its notation to θ^*_{m}. Also, we know that $\Delta\omega$ is a constant, so Eq. 2.60 becomes:

$$\Delta\omega = K_c^{**}\, \mathbf{E}[\sin(\theta_{\text{s}} - \theta^*_{\text{m}} + c_{\text{ext}}\xi_{\text{ext}})]\ . \tag{2.62}$$

Applying the definition of expected value, Eq. 2.61 has an integral form of:

$$\mathbf{E}[\sin(\theta_{\mathrm{s}} - \theta^*_{\mathrm{m}} + c_{\mathrm{ext}}\xi_{\mathrm{ext}})] \tag{2.63a}$$

$$= \int_{-\infty}^{\infty} d\theta^*_{\mathrm{m}} P(\theta^*_{\mathrm{m}}) \sin(\theta_{\mathrm{s}} - \theta^*_{\mathrm{m}}) \tag{2.63b}$$

$$\times \int_{-\infty}^{\infty} d\xi_{\mathrm{ext}} P(\xi_{\mathrm{ext}}) \cos(c_{\mathrm{ext}}\xi_{\mathrm{ext}}) \tag{2.63c}$$

$$+ \int_{-\infty}^{\infty} d\theta^*_{\mathrm{m}} P(\theta^*_{\mathrm{m}}) \cos(\theta_{\mathrm{s}} - \theta^*_{\mathrm{m}}) \tag{2.63d}$$

$$\times \int_{-\infty}^{\infty} d\xi_{\mathrm{ext}} P(\xi_{\mathrm{ext}}) \sin(c_{\mathrm{ext}}\xi_{\mathrm{ext}}). \tag{2.63e}$$

Following the derivation of similar integrals in Eq. 2.47 and 2.53, the above equation Eq. 2.63 becomes:

$$\mathbf{E}[\sin(\theta_{\mathrm{s}} - \theta^*_{\mathrm{m}} + c_{\mathrm{ext}}\xi_{\mathrm{ext}})] \tag{2.64a}$$

$$= \int_{-\infty}^{\infty} d\theta^*_{\mathrm{m}} P(\theta^*_{\mathrm{m}}) \sin(\theta_{\mathrm{s}} - \theta^*_{\mathrm{m}}) \tag{2.64b}$$

$$\times \int_{-\infty}^{\infty} d\xi_{\mathrm{ext}} P(\xi_{\mathrm{ext}}) \cos(c_{\mathrm{ext}}\xi_{\mathrm{ext}}) \tag{2.64c}$$

$$= \mathbf{E}[\sin(\theta_{\mathrm{s}} - \theta^*_{\mathrm{m}})] \times \mathbf{E}[\sin(\theta_{\mathrm{s}} - \theta_{\mathrm{m}} + c_{\mathrm{ext}}\xi_{\mathrm{ext}})] \tag{2.64d}$$

$$= c_{\mathrm{ext}} \exp\left[- \frac{(c_{\mathrm{ext}}\sigma_{\mathrm{ext}})^2 + (c_{\mathrm{int}}\sigma_{\mathrm{int}})^2}{2} \right]. \tag{2.64e}$$

Finally, we substitute Eq. 2.64 into 2.62, to find the critical coupling constant K_c^{**} with both external and internal noise:

$$K_c^{**} = \frac{|\Delta\omega|}{c_{\mathrm{ext}}} \exp\left[\frac{(c_{\mathrm{ext}}\sigma_{\mathrm{ext}})^2 + (c_{\mathrm{int}}\sigma_{\mathrm{int}})^2}{2} \right]. \tag{2.65}$$

2.4 Cost Analysis

We assume that the cost of operating a circadian clock results from the (absolute) phase mismatch between the circadian oscillator and the solar cycle oscillator. We define the cost function as $1 - \textit{cosine}$ of the phase mismatch, averaged over all integration steps:

$$C = \frac{1}{N_i} \sum_{\mathrm{i}}^{N_i} \left[1 - \cos\left(\theta_{\mathrm{s,i}} - \theta_{\mathrm{m,i}} \right) \right], \tag{2.66}$$

where N_i is the total number of integration steps. For a strongly coupled system (large K), the phase mismatch between the two oscillators can become very small, and as a result, we

can expand the *sine* function in Eq. 2.4:

$$\sin(\theta_{\rm s} - \theta_{\rm m}) \approx \theta_{\rm s} - \theta_{\rm m} = \Delta\theta, \qquad \Delta\theta \ll 1 \ . \tag{2.67}$$

Similarly, a strongly coupled system is synchronized in frequency as well, so Eq. 2.4 becomes:

$$\omega_{\rm s} = \omega_{\rm m} + K\sin(\theta_{\rm s} - \theta_{\rm m}) \approx \omega_{\rm m} + K\Delta\theta, \quad \Delta\omega = \omega_{\rm s} - \omega_{\rm m}, \quad \Delta\theta = \frac{\Delta\omega}{K} \ . \tag{2.68}$$

Thus the cost function Eq.2.66 can be written as:

$$C_{\rm approx} \approx \frac{1}{N_i}\sum_{\rm i}^{N_i}\left[1 - \cos\left(\Delta\omega/K\right)\right], \qquad K \gg K_c. \tag{2.69}$$

If the model is stochastic, each computation will produce a different trajectory of the circadian oscillator. We take the expectation value of the $1 - cosine$ of phase mismatch for multiple phase trajectories at each time step, which is $\langle(1 - \cos\left(\theta_{\rm s,i} - \theta_{\rm m,i}\right)\rangle$. Then we calculate the cost in terms of the expectation value:

$$C_* = \frac{1}{N_i}\sum_{\rm i}^{N_i}\langle(1 - \cos\left(\theta_{\rm s,i} - \theta_{\rm m,i}\right)\rangle. \tag{2.70}$$

Finally, we also want to know the cost of an organism having no circadian clock as well, which can be defined by:

$$C_0 = \frac{1}{N_i}\sum_{\rm i}^{N_i}[1 - \cos(\theta_{\rm s,i})]. \tag{2.71}$$

Chapter 3

Result and Discussion

Throughout this entire chapter, we will perform all of our analysis with the intrinsic frequency of the solar-cycle oscillator set at $\omega_{\mathrm{s}} = \frac{2\pi}{24}\frac{\mathrm{rad}}{\mathrm{hours}}$. This setting guarantees the solar-cycle oscillator makes 1 complete revolution for every 24 hours. Any integration of an ordinary differential equation or stochastic differential equation is discretized with a time step of $\Delta t = 0.01$ hour.

3.1 Deterministic Model

3.1.1 Deterministic Time-courses

We compute the phase of the solar-cycle oscillator in Eq. 2.3 and the phase of the circadian clock in Eq. 2.4 under three different coupling conditions. This computation is done by using the deterministic leapfrog integrator in Eq. 2.14. Later we take the result of integration to compute the time-courses of each oscillator in Eq. 2.5. The time-courses of deterministic circadian clocks as a result of the computation are shown in Fig. 3.1.

We categorize the sample circadian clocks shown in Fig. 3.1 into three groups based on their time-courses. Firstly, we categorize the circadian clock in Fig. 3.1a as a 'bad' circadian clock because its oscillation frequency is not synchronized with the solar-cycle oscillator. Research has shown that a human with 24-hour circadian clock experiences deepest sleep from 2:00am to 4:00am [16]. We can imagine if a person has a similar high-frequency circadian clock as shown in Fig. 3.1a, his time frame to achieve deep sleep will be shortened and this might affect his health. Hence, we will expect that the operational cost of a 'bad' circadian clock is higher than the other examples in Fig. 3.1.

The other two circadian clocks in Fig. 3.1 are frequency synchronized with the solar-cycle oscillator; one is shown in Fig. 3.1b with $K = 1.0\ \Delta\omega$ and the other one is shown in Fig. 3.1c with $K = 3.0\ \Delta\omega$. The circadian clock from Fig. 3.1b is categorized as a 'good' circadian clock because its frequency is synchronized with the solar-cycle oscillator. An organism with possession of such internal circadian clock can fully utilize the 24-hour solar cycle to organize its physiological and mental activities. However, this clock has larger

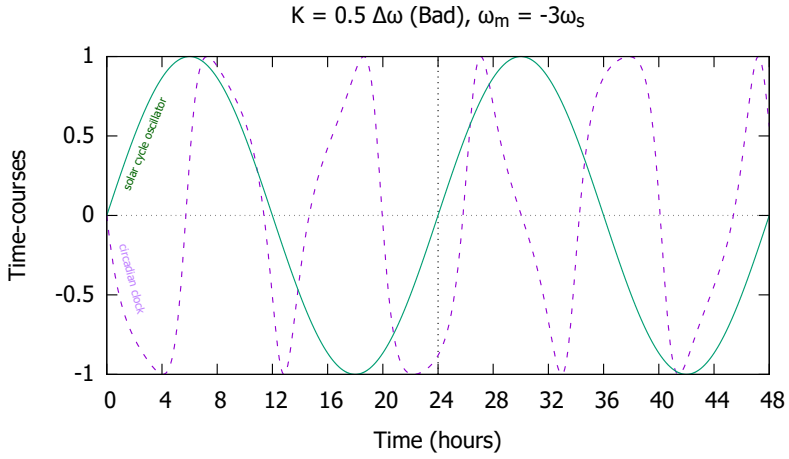

(a) Bad Circadian Clock

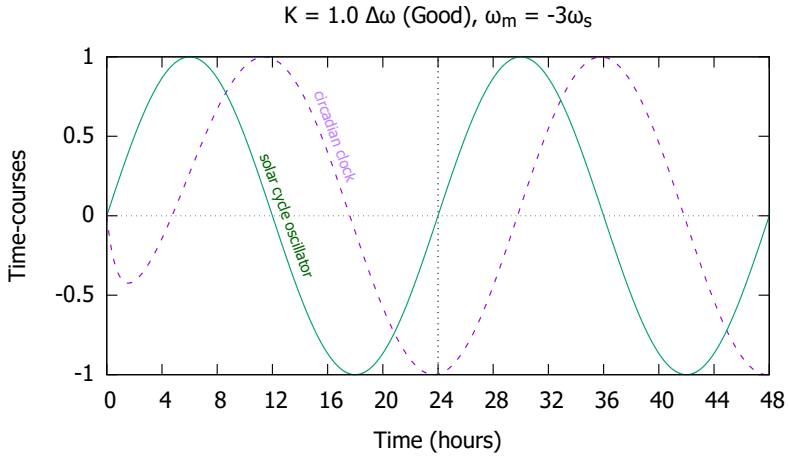

(b) Good Circadian Clock

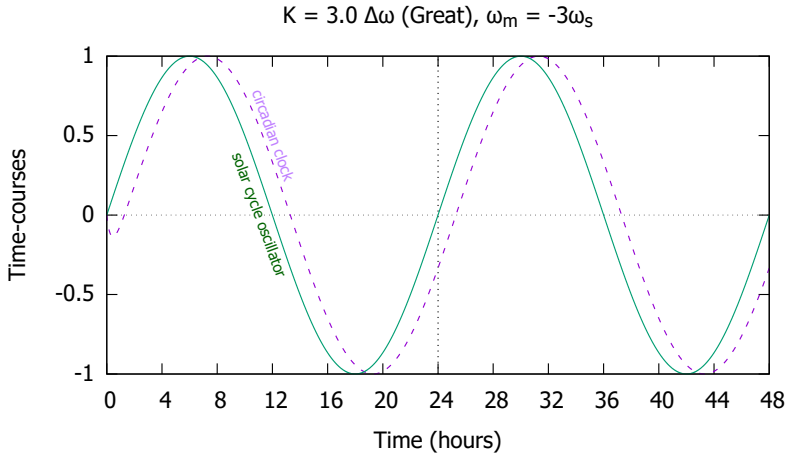

(c) Great Circadian Clock

Figure 3.1: Time-courses of deterministic circadian clock computed via Eq. 2.4 and 2.5 with coupling constants: a) $K = 0.5\ \Delta\omega$, b) $K = 1.0\ \Delta\omega$ and c) $K = 3.0\ \Delta\omega$. We set parameters to $\omega_{\mathrm{s}} = \frac{2\pi}{24}$, $\omega_{\mathrm{m}} = -3.0\ \omega_{\mathrm{s}}$, $B_{\mathrm{m}} = 1$ and $B_{\mathrm{s}} = 1$.

phase mismatch compares to the 'great' clock in Fig. 3.1c. The 'great' circadian clock in Fig. 3.1c closely tracks the solar-cycle oscillator. An organism with such circadian clock not only can utilize the 24-hour solar time but also can capitalize environmental resource such as sunlight. We expect that the operating cost of the 'great' clock will be lower than the 'good' clock.

3.1.2 Critical Coupling

We derive the critical coupling constant K_c in Eq. 2.29 as the coupling constant beyond which ($K \geq K_c$) a circadian clock achieves frequency synchronization with the solar-cycle oscillator, as defined in Eq. 2.27. This can be tested by simulating multiple circadian clocks with different intrinsic frequencies ω_{m} and subsequently increasing coupling constant K to observe whether the oscillation frequency $\dot{\theta_{\mathrm{m}}}$ of a circadian clock reaches steady state after K surpasses a threshold value. The result of this computation is shown in Fig. 3.2. Five

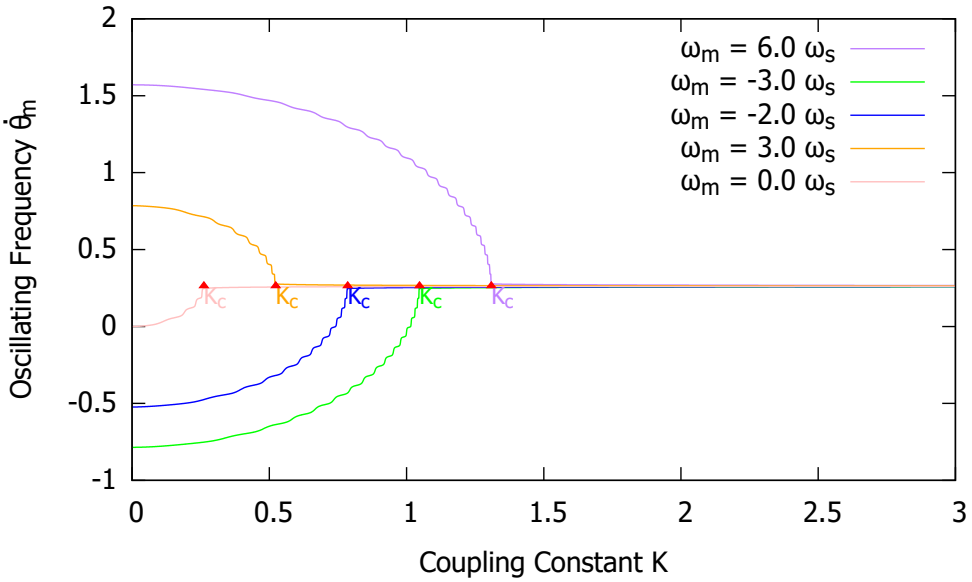

Figure 3.2: Oscillating frequencies $\dot{\theta}_{\mathrm{m}}$ of circadian clocks with different intrinsic frequency ω_{m} as a function of coupling constant K. The oscillation frequency $\dot{\theta_{\mathrm{m}}}$ of circadian clock is calculated with Eq. 2.4. ▲ marks the value of K when $\dot{\theta_{\mathrm{m}}}$ reaches steady state.

circadian clocks are simulated and their oscillation frequency reaches steady state after K surpasses K_c, which K_c is marked on the plot with ▲. We can simulate more circadian clocks in this way to extract data of K_c as a function of ω_{m} to test the validity of Eq. 2.29.

The critical coupling constants K_c are extracted based on the above method. Figure 3.3 shows K_c as a function of intrinsic frequency ω_{m}. The data in Fig. 3.3 is fitted to Eq. 2.29 and the fitting shows agreement between extracted data and theoretical prediction in Eq. 2.29. We observe there is a proportionality between intrinsic frequency ω_{m} and critical coupling constant K_c. Intuitively, we can understand that if a circadian clock has an intrinsic fre-

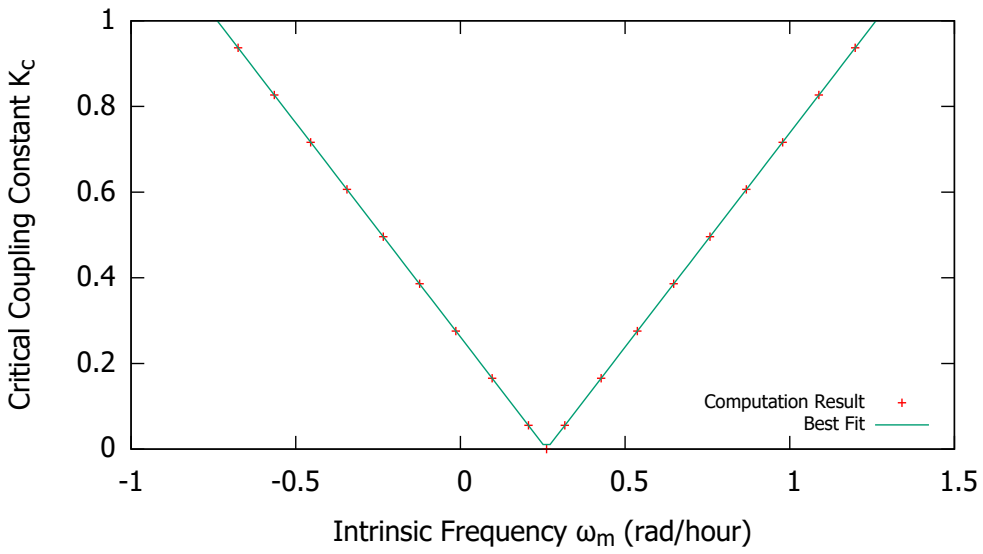

Figure 3.3: Critical coupling constant K_c as a function of intrinsic frequency of circadian clock ω_{m}. The computation result is fitted to $K_c = |\omega_{\mathrm{s}} - \omega_{\mathrm{m}}|$ (Eq. 2.29) with fitting coefficient $\omega_{\mathrm{s}} = 0.2618 \approx \frac{2\pi}{24}$ (rad/hour).

quency ω_{m} further apart from the solar cycle frequency ω_{s}, such circadian clock requires larger coupling constant to reach frequency synchronization with the solar-cycle oscillator.

3.1.3 Cost Analysis

Figure 3.4 shows the operational cost of a circadian clock (2.66) as a function of coupling constant K. The operational costs of the three circadian clocks in Fig. 3.1 are labeled with their name in Fig. 3.4. As expected, the bad clock has highest cost of operation among the three and the great clock has the least operational cost.

The colored dashed lines signify the start of significant drop in the operational cost of the circadian clock with the corresponding color. Coincidentally, each dashed line also marks the location of theoretical critical coupling constant K_c calculated using Eq. 2.29 for each circadian clock. As the circadian clock shifts to achieve phase synchronization, its operational cost is significantly reduced. The significant drop in cost is more evident on the log-scale plot in Fig. 3.4b, where the cost of operation decreases in a straight line, showing an exponential drop in cost.

The cost of operating no circadian clock (2.71) (an organism performs tasks whenever it likes) is the horizontal black line in Fig.3.4. The cost of operating no circadian clock is maximal, but also equal to the cost of operating a clock that cannot frequency-synchronize with the solar-cycle oscillator. Fig. 2.66 shows that the cost of operating no circadian clock is about the same as operating a bad clock. The operational cost of a circadian clock is

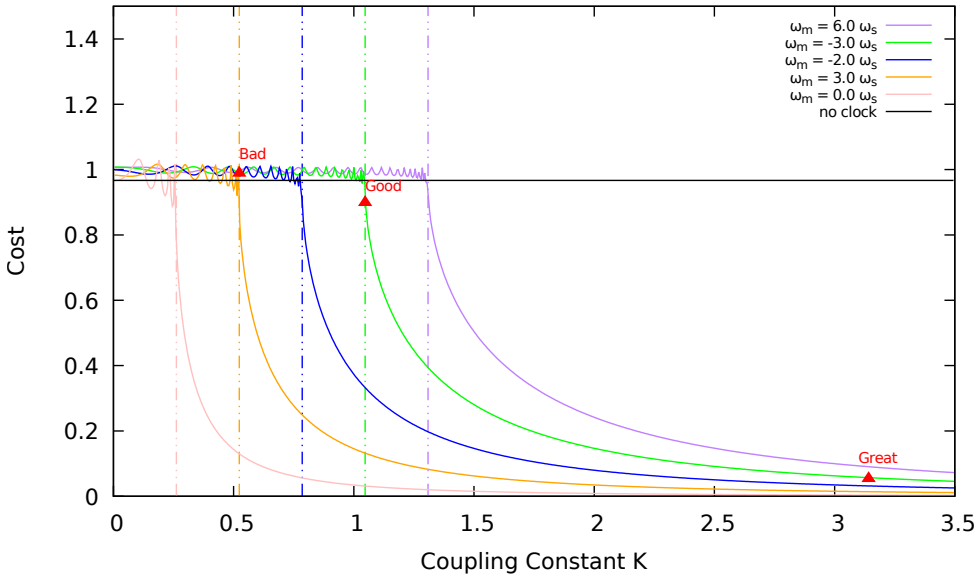

(a) Linear Scale

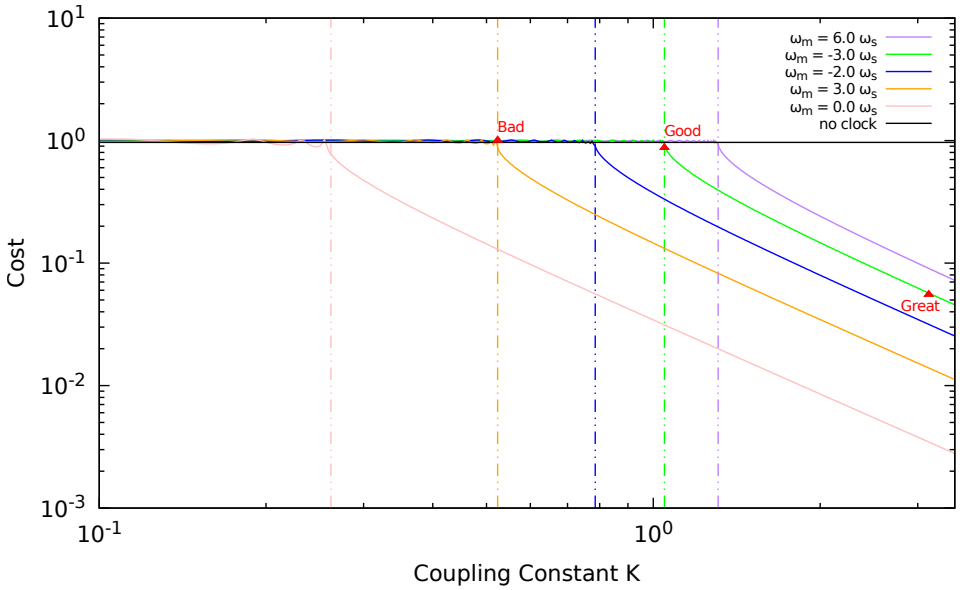

(b) Log Scale

Figure 3.4: Operational cost (2.66) as a function of coupling constant for circadian clocks with various intrinsic frequencies ω_{m}. a) linear scale; b) log scale. ▲ mark the cost of operating circadian clocks shown in Fig. 3.1.

low only when the clock is able to reach frequency synchronization, otherwise it is just as optimal as operating no circadian clock.

We can compare the cost of operating circadian clock with $\omega_{\mathrm{m}} = 6.0\ \omega_{\mathrm{s}}$ (purple line) and $\omega_{\mathrm{m}} = -3.0\ \omega_{\mathrm{s}}$ (green line) in Fig. 3.4. A circadian clock with intrinsic frequency closer to the solar cycle frequency (green line in this case) will have lower operating cost when it is frequency-synchronized with the solar cycle oscillator under the same coupling constant. That shows the operational cost of a circadian clock is also proportional to its intrinsic frequency ω_{m}. However this is only true when the circadian clock is at frequency synchronization with the solar-cycle oscillator and only valid when we perform comparison under the same coupling constant. If a circadian clock is already frequency-synchronized, its cost of operation is lower if its intrinsic frequency is closer to the solar cycle frequency.

There are some small oscillations in the cost of operation when the circadian clock is not frequency synchronized, stemming from the *cosine* function in Eq. 2.66. Further study is needed to understand the physical reason for these.

3.2 Stochastic Model with Internal Noise

3.2.1 Stochastic Time-courses

The phase of a circadian clock with internal noise can be obtained by integrating the stochastic differential equation in Eq. 2.6 with stochastic leapfrog integrator in Eq. 2.24. The time-courses of a circadian clock with internal noise is computed by Eq. 2.5. Four circadian clocks are shown in Fig. 3.5, each clock with a different coupling condition. Even though the time-courses of each clock are noisy, their periodic motion is still intelligible.

Similar to the last subsection, we categorize the circadian clocks in Fig. 3.5 according to their frequency synchronization with the solar-cycle oscillator. The circadian clock Fig. 3.5a is a 'bad' circadian clock as previously discussed in § 3.1.1. In Fig. 3.5b, the circadian clock has $K = 1.0\ \Delta\omega$ equal to the critical coupling constant for the deterministic model. However, such a clock is not synchronized with the solar-cycle oscillator due to internal noise. This circadian clock neared synchronization in the first 24 hours but failed immediately afterward (Fig. 3.5b). We categorize this circadian clock as 'good' because it has the same coupling constant as the good circadian clock in Fig. 3.1b. A 'better' circadian clock (Fig. 3.5c) is frequency synchronized with the solar-cycle oscillator, but without phase synchronization. Then we have a 'great' circadian clock (Fig. 3.5d) tracks the solar-cycle oscillator closely. Comparing Fig. 3.5b with 3.1b, it is intuitive to expect that operating a stochastic circadian clock will yield higher operational cost compared to a deterministic clock if the circadian clock is frequency-synchronized with the solar cycle oscillator in a deterministic environment.

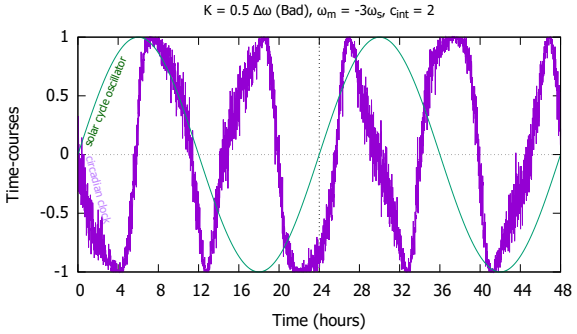

(a) Bad Circadian Clock

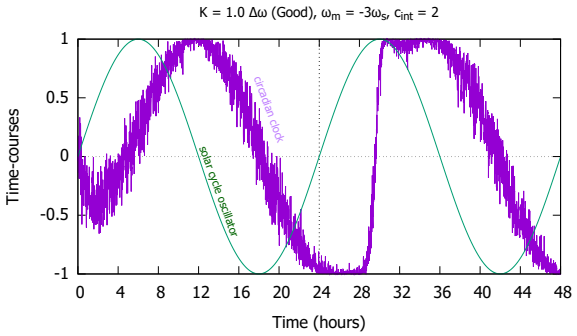

(b) Good Circadian Clock

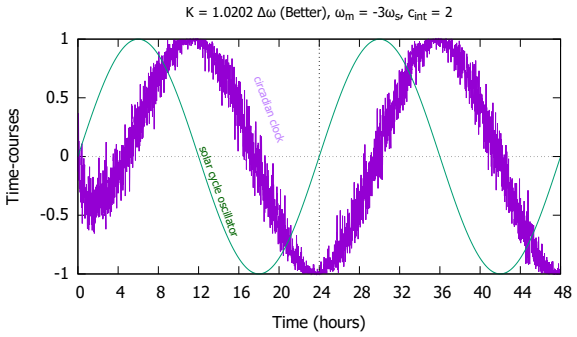

(c) Better Circadian Clock

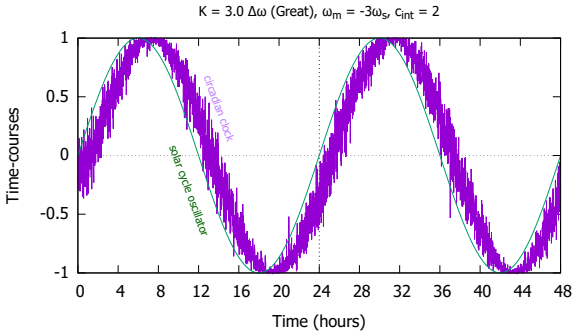

(d) Great Circadian Clock

Figure 3.5: Time-courses of stochastic circadian clock with internal noise computed via Eq. 2.5 and 2.6 with coupling constants: a) $K = 0.5\ \Delta\omega$, b) $K = 1.0\ \Delta\omega$, c) $K = 1.0202\ \Delta\omega$ and d) $K = 3.0\ \Delta\omega$. In all panels, $\omega_{\rm s} = \frac{2\pi}{24}$, $c_{\rm int} = 2.0$, $\omega_{\rm m} = -3.0\ \omega_{\rm s}$, $B_{\rm m} = 1$ and $B_{\rm s} = 1$.

3.2.2 Critical Coupling

The oscillation frequency of a circadian clock with internal noise is described by Eq. 2.6. We assume that the oscillation frequency of a circadian clock with internal noise will reach steady state when $K \geq K^*_{\text{c,int}}$. Based on this assumption we derive the equation of critical coupling constant for the stochastic model with internal noise. Figure 3.6 shows tests of multiple circadian clocks under different noise strengths c_{int} with progressively increasing coupling constants to determine when the clock's oscillation frequency reaches steady state.

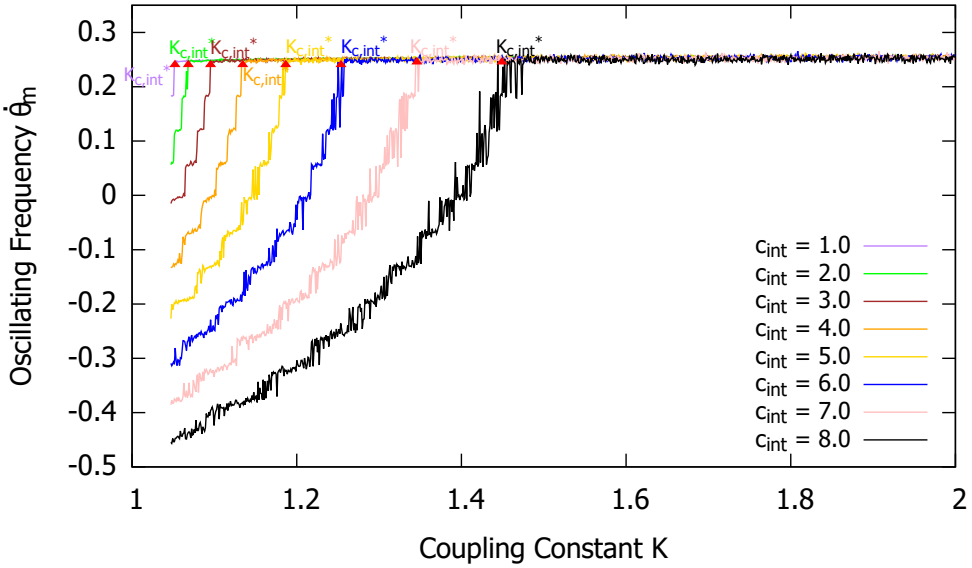

Figure 3.6: Oscillating frequencies $\dot{\theta}_{\text{m}}$ of stochastic circadian clocks with internal noise as a function of coupling constant K. The intrinsic frequency of the circadian clock is $\omega_{\text{m}} = -3.0\ \omega_{\text{s}}$. The oscillation frequency $\dot{\theta_{\text{m}}}$ of the circadian clock is calculated with Eq. 2.6. ▲ marks the critical K where $\dot{\theta_{\text{m}}}$ reaches steady state.

Figure 3.6 shows that the oscillation frequency of a circadian clock with internal noise indeed reaches steady state after surpassing a threshold coupling constant $K^*_{\text{c,int}}$.

The critical coupling constant increases with the noise strength c_{int}. ▲ mark the critical coupling constants $K^*_{\text{c,int}}$ of circadian clocks with internal noise of varying strengths. Figure 3.7 shows empirical $K^*_{\text{c,int}}$ as a function of noise strength c_{int}, fitted to Eq. 2.48, with strong agreement between data and our theoretical prediction. We have set $|\Delta\omega| = |\frac{2\pi}{24} - -\frac{6\pi}{24}| = \frac{\pi}{3}$ (rad/hours) and $\sigma_{\text{int}} = \sqrt{\Delta t} = \sqrt{0.01}$ in our calculations. The fit parameters are $|\Delta\omega| = 1.047$ and $\sigma_{\text{int}} = 0.1005$. The fit parameters agree with our theory, where $|\Delta\omega| = 1.047 \approx \frac{\pi}{3}$ and $\sigma_{\text{int}} = 0.1005 \approx \sqrt{0.01}$. The critical coupling constant grows exponentially with the noise strength, confirming that frequency synchronization is more difficult when the system is more noisy.

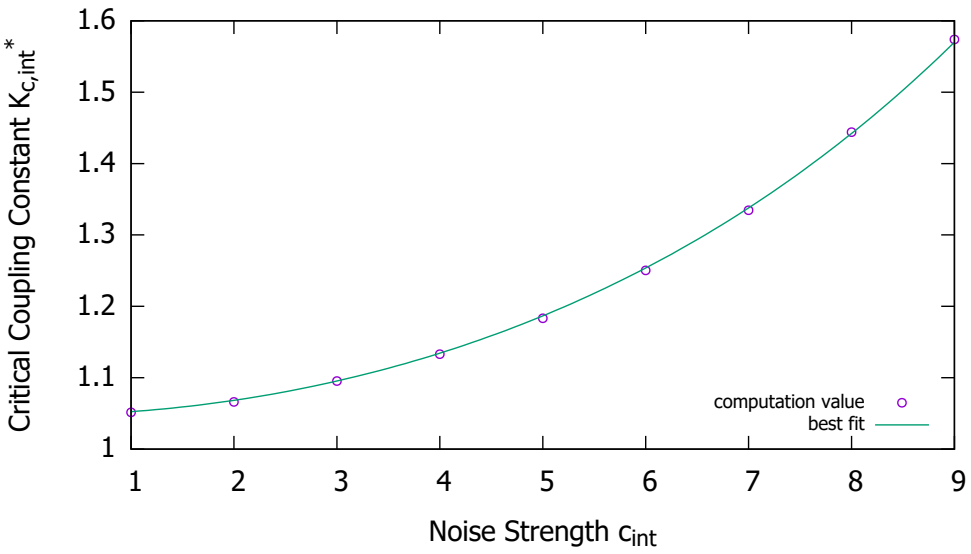

Figure 3.7: Critical coupling constant $K^*_{\mathrm{c,int}}$ as a function of internal noise strength c_{int}. The numerical result (purple open circles) is fitted to Eq. 2.48 (teal curve). The fit parameters are $|\Delta\omega| = 1.047$ (rad/hour) and $\sigma_{\mathrm{int}} = 0.1005$ (rad/hour).

3.2.3 Cost Analysis

Figure 3.8 shows the operational cost of a circadian clock with internal noise (Eq. 2.70), averaged over many trajectories, as a function of the coupling constant. A major distinction between stochastic and deterministic models is the increase in operational cost for circadian clocks that reach frequency synchronization. The cost of operating no circadian clock is the same for both models. From the deterministic model, the good circadian clock has the cost of operation below the cost of operating no circadian clock. However, the good clock is not frequency synchronized with the solar-cycle oscillator under the stochastic model, and its cost of operation is about the same as operating a bad clock or no clock. Nevertheless, if a deterministic circadian clock is not frequency synchronized with the solar-cycle oscillator, there is no noticeable cost increase when the same clock is operated within stochastic environment (Fig. 3.8a and 3.4a). By contrast, the operational cost of a circadian clock increases with the internal noise strength when the clock is frequency synchronized. Fig. 3.5 shows some large-magnitude random jumps in the time-courses of a circadian clock with internal noise. We also observe that as increasing noise strength, these jumps are larger in magnitude and occur more often. From our observation based on the time course, we believe these jumps are the source of high operational cost in a stochastic circadian clock with internal noise.

Comparing Fig. 3.8b with 3.4b reveals another distinction between stochastic and deterministic models. For the stochastic model with internal noise, the drop in cost when a

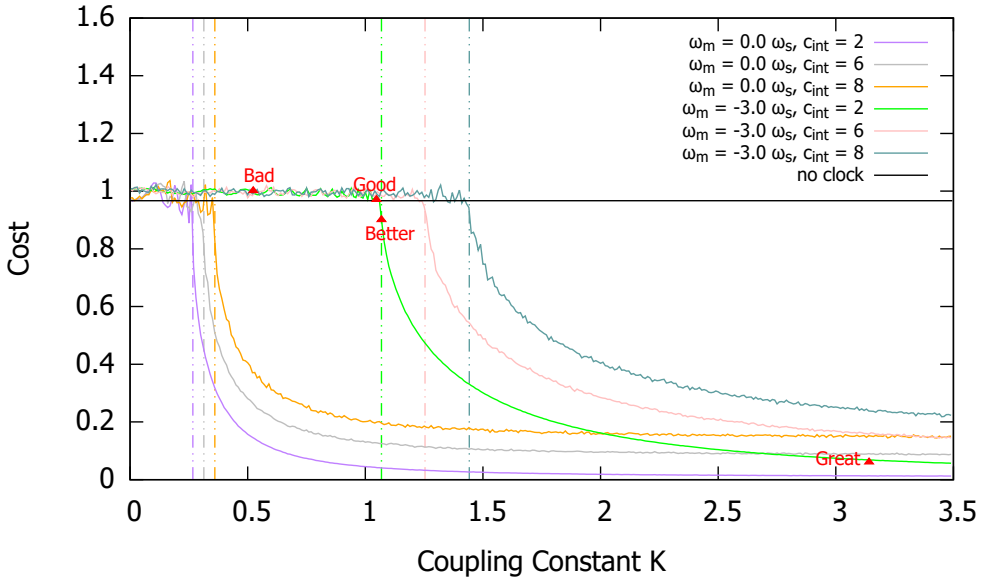

(a) Linear Scale

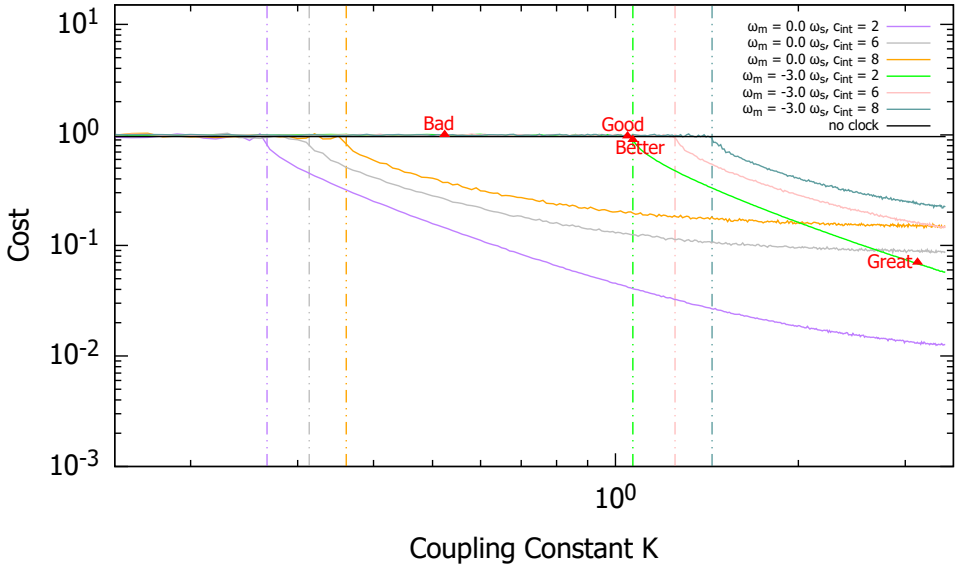

(b) Log Scale

Figure 3.8: Operational cost (2.70) as a function of coupling constant for stochastic circadian clocks with internal noise ξ_{int} and different intrinsic frequency ω_{m}, averaged over 10 trials. a) linear scale and b) log scale. ▲ mark the cost of operating circadian clocks shown in Fig. 3.5.

circadian clock shifts from frequency synchronization to phase synchronization is not exponential (a straight line on log scale). Moreover, the rate of cost decrease slows as the coupling constant increases (e.g., orange line in Fig. 3.8b). This slow-down occurs when the phase mismatch between the two oscillators is dominated by the added noise. We note that as the coupling constant increases, the periodic motion of the circadian clock more closely tracks the solar-cycle oscillator, but the noise strength remains the same. Thus the operational cost of a circadian clock reaches an asymptotic value at high coupling constant, as the result of internal noise.

Unlike in the deterministic model, the operational cost of a circadian clock with internal noise depends on its intrinsic frequency, noise strength, and coupling constant. Fig. 3.8a shows that the operational cost of a noisy oscillator can be higher than that of a noiseless circadian clock with greater intrinsic frequency mismatch. (orange line and green line crossing at high coupling constant). The presence of internal noise (in orange line) leads to non-zero limiting asymptotic operational cost. This is not observed in the deterministic model, where the operating cost is always higher for the circadian clock with greater intrinsic frequency mismatch.

3.3 Stochastic Model with External Noise

3.3.1 Stochastic Time-courses

The phase of a stochastic circadian clock with external noise can be obtained by integrating the SDE in Eq. 2.8 with stochastic integrator in Eq. 2.25. Figure 3.9 shows time-courses of four circadian clocks, each with a different coupling constant. At first glance, the time-courses of circadian clock with external noise look more similar to the deterministic model than the stochastic model with internal noise.

The bad circadian clock (Fig. 3.9a) closely resembles the bad circadian clock from the deterministic model in Fig. 3.1a. The good circadian clock (Fig. 3.9b) appears different from the deterministic model due to external noise. The better circadian clock (Fig. 3.9c) is frequency synchronized with the solar-cycle oscillator, similar to the good circadian clock from the deterministic model but with a larger coupling constant. The great circadian clock (Fig. 3.9c) appears similar to the great clock from the deterministic model.

The biggest difference between the circadian clock with internal noise and external noise is the time-courses of circadian clock with external noise are not noisy. The external noise is added inside the coupling function, affecting the circadian clock's tracking ability to the solar-cycle oscillator. The dynamics of the stochastic time-delay model in Eq. 2.12 requires further study to explain the smoothness of the time-courses even though noise is implemented.

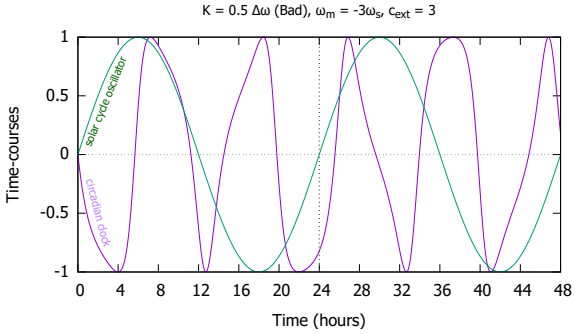

(a) Bad Circadian Clock

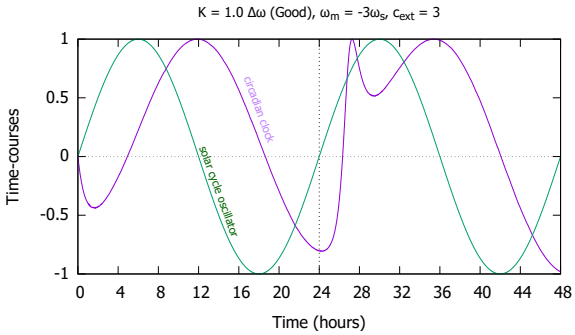

(b) Good Circadian Clock

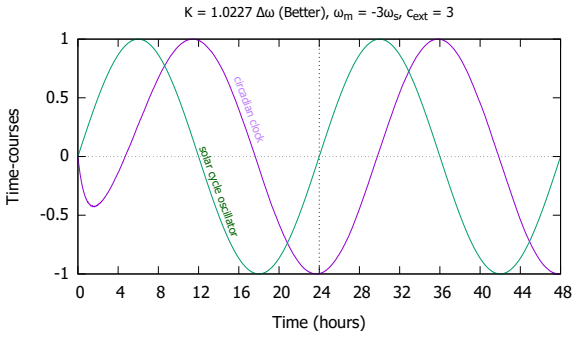

(c) Better Circadian Clock

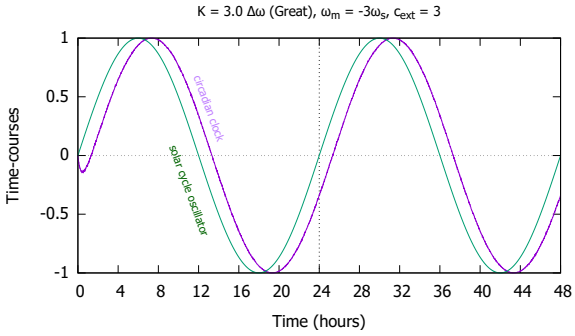

(d) Great Circadian Clock

Figure 3.9: Time-courses of stochastic circadian clocks with external noise computed via Eq. 2.5 and 2.8, with coupling constants: a) $K = 0.5\ \Delta\omega$, b) $K = 1.0\ \Delta\omega$, c) $K = 1.0227\ \Delta\omega$ and d) $K = 3.0\ \Delta\omega$. In all sub-panels, $\omega_{\rm s} = \frac{2\pi}{24}$, $c_{\rm ext} = 3.0$, $\omega_{\rm m} = -3.0\ \omega_{\rm s}$, $B_{\rm m} = 1$ and $B_{\rm s} = 1$.

3.3.2 Critical Coupling

To see whether the oscillation frequency $\dot{\theta}^*_{\mathrm{m,ext}}$ of a circadian clock with external noise will reach steady state after K surpasses $K^*_{\mathrm{c,ext}}$, we compute the oscillation frequency in Eq. 2.8 as a function of coupling constant K (Fig. 3.10).

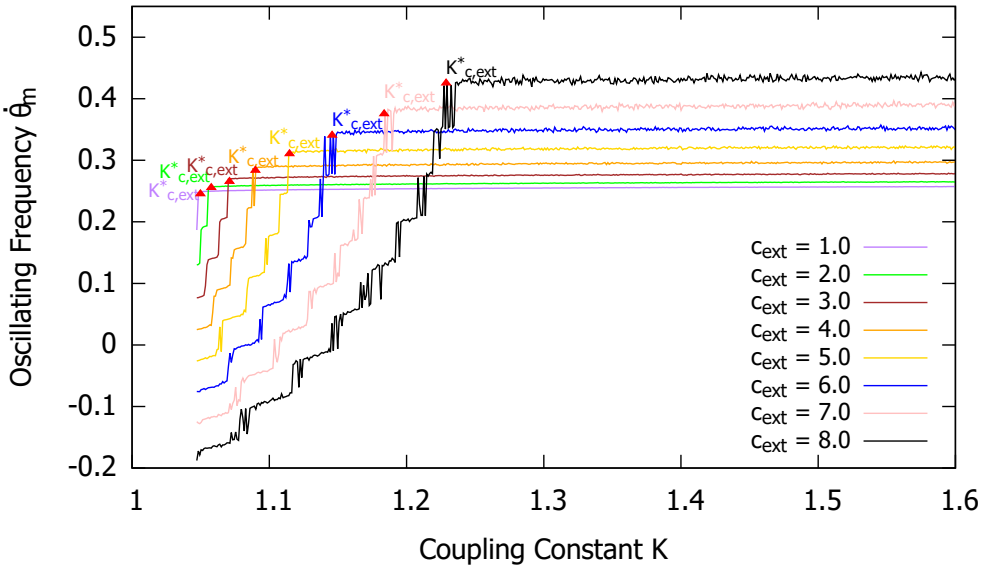

Figure 3.10: Oscillation frequencies $\dot{\theta}_{\mathrm{m}}$ of stochastic circadian clocks with external noise, as a function of coupling constant K. The intrinsic frequency of the circadian clock is $\omega_{\mathrm{m}} = -3.0\,\omega_{\mathrm{s}}$. The oscillation frequency $\dot{\theta}_{\mathrm{m}}$ of the circadian clock is calculated with Eq. 2.8. ▲ mark the value of K when $\dot{\theta}_{\mathrm{m}}$ reaches steady state.

In this case, the oscillation frequency of a circadian clock does reach to a steady state value, but that limiting frequency is also influenced by the noise strength c_{ext}. The markers ▲ in Fig. 3.10 shows the location of K when the limit is reached, which is also the location of the critical coupling constant $K^*_{\mathrm{c,ext}}$ in Eq. 2.49. Figure 3.10 shows that a circadian clock has a strong-coupling frequency that differs from the solar-cycle frequency ω_{s}. This differs from the time-courses of the great circadian clock in Fig. 3.9, which is clearly synchronized to the solar-cycle frequency. This behavior may arise from the time-delay equation in Eq. 2.12.

Our derived theory in Eq. 2.49 and 2.59 do not agree with the above data, but we can still examine the relationship between external noise strength and critical coupling constant $K^*_{\mathrm{c,ext}}$. Figure 3.11 shows the critical coupling constant as a function of external noise strength c_{ext} in Eq. 2.55.

Clearly the theoretical prediction disagrees with the numerical data. We use physical intuition to guess a functional form,

$$K^*_{\mathrm{c,ext}} \sim |\Delta\omega| \, \exp\left[\frac{(c_{\mathrm{ext}}\sigma_{\mathrm{ext}})^2}{4}\right] . \tag{3.1}$$

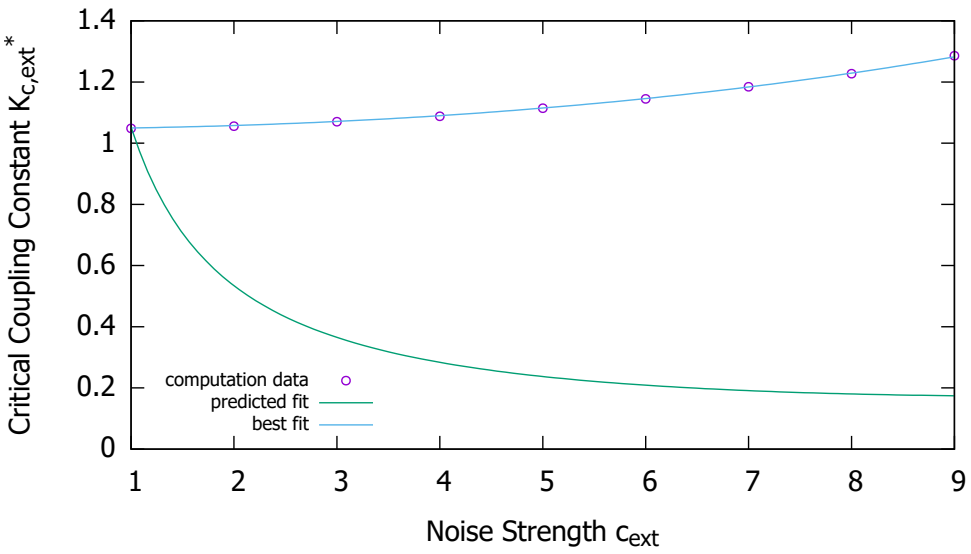

Figure 3.11: Critical coupling constant $K^*_{\mathrm{c,ext}}$ as a function of external noise strength c_{ext}. The numerical results are fitted to Eq. 2.59 and 3.1. The parameters obtained from fitting to Eq. 3.1 are $|\Delta\omega| = 1.047$ (rad/hour) and $\sigma_{\mathrm{ext}} = 0.1008$ (rad).

The data in Fig. 3.11 is fitted to Eq. 3.1. We have set $|\Delta\omega| = \frac{\pi}{3}$ and $\sigma_{\mathrm{ext}} = \sqrt{\Delta t} = \sqrt{0.01}$ in the computation. The fit parameters are $|\Delta\omega| = 1.047$ (rad/hour) and $\sigma_{\mathrm{ext}} = 0.1008$. These fit parameters are very close to the parameters we have obtained from fitting to data extracted for stochastic model with internal noise in Fig. 3.7 and close to the parameters in our calculations. Comparing Eq. 2.48 and 3.1, the empirical fit implies that at the same noise strength and frequency mismatch, internal noise has a larger influence on the critical coupling constant than external noise does, by a factor of e^2.

3.3.3 Cost Analysis

The operational cost of a circadian clock with external noise is given by Eq. 2.70. Following similar computation from the previous section § 3.2.3, Fig. 3.12 shows the operational cost of circadian clocks with external noise as a function of coupling constant K.

Interestingly, Fig. 3.12 looks very similar to Fig. 3.4. The operational cost of the four circadian clocks in Fig.3.9 are marked by ▲ and explicitly labeled. The bad and good circadian clocks in Fig. 3.9 are not frequency synchronized with the solar-cycle oscillator, hence their operational cost is higher than the better and great circadian clocks. This is consistent with the stochastic model with internal noise. Again, there is no noticeable cost increase upon adding external noise to deterministic circadian clocks that already failed to achieve frequency synchronization with the solar-cycle oscillator. Comparing the cost of operating a bad circadian clock across (Figs. 3.4a, 3.8a and 3.12a). However, a circadian

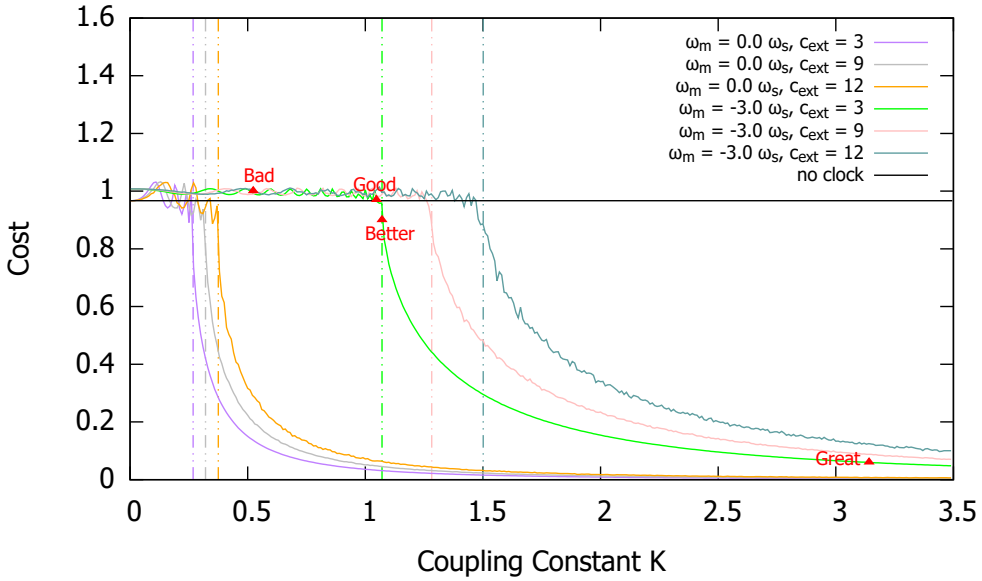

(a) Linear Scale

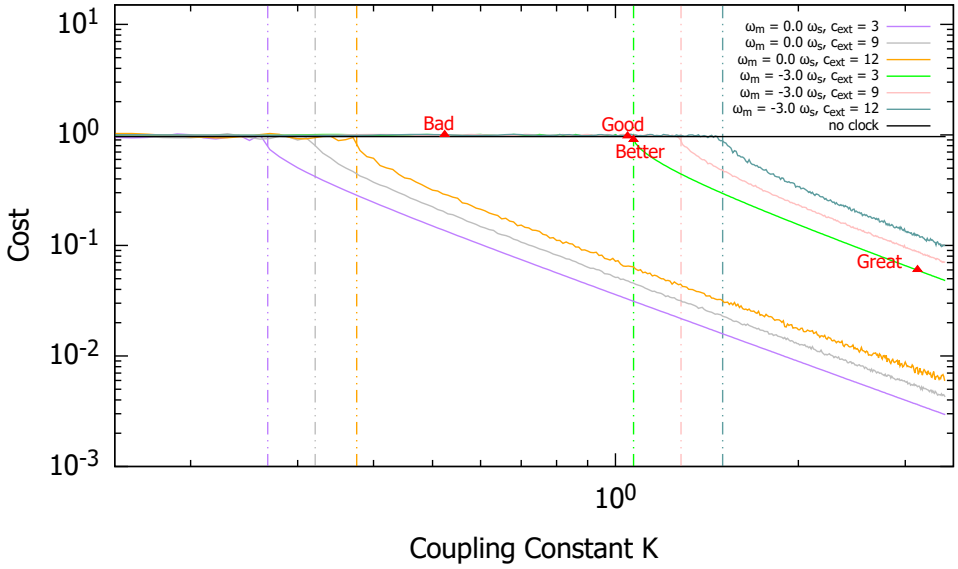

(b) Log Scale

Figure 3.12: Operational cost (Eq. 2.70), averaged over 10 trajectories, as a function of coupling constant for stochastic circadian clocks with varying external noise strengths c_{ext} and intrinsic frequencies ω_{m}. a) Linear scale and b) log scale. ▲ mark the cost of operating circadian clocks shown in Fig. 3.9.

clock that when deterministic is frequency synchronized will incur higher costs upon the introduction of either internal or external noise.

The colored dashed lines in Fig. 3.12 represent the critical coupling constants $K^*_{\mathrm{c,ext}}$ (Eq. 3.1). The operational cost of circadian clocks with external noise is also plotted on log-scale axes in Fig. 3.8b. The significant drop in operational cost of circadian clocks occurs along the shift from frequency synchronization to phase synchronization with the solar-cycle oscillator. And the significant drop is linear on the log plot, indicating exponential decrease, again resembling the deterministic model and differing from the stochastic model with internal noise.

Contrasting with the internal-noise case, there is no non-zero limiting asymptotic operational cost because the time-courses of circadian clock with external noise is smooth. As the external noise strength does affect the cost of operation as previously discussed, overall Fig. 3.12 shows a mixture of properties from the deterministic model and from the stochastic model with internal noise.

3.4 Stochastic Model with Internal and External Noise

3.4.1 Stochastic Time-courses

The phase of a circadian clock with internal and external noise is obtained by integrating the SDE in Eq. 2.13 with stochastic leapfrog integrator in Eq. 2.26. Figure 3.13 shows the time-courses of four circadian clocks with internal and external noise. The categorization of circadian clocks with internal and external noise in Fig. 3.13 is similar to Fig. 3.5 in § 3.1.1.

There are many similarities between the time-courses of circadian clocks in Fig. 3.13 and the time-courses of circadian clocks with internal noise in Fig. 3.5. However, the periodic motion of a good circadian clock with internal and external noise is different than the good clock with only internal noise. Figure 3.13b shows a small oscillation in time-courses between $t = 40$ and 48. These kinds of small oscillations in time-courses are only observed from the stochastic model with external noise, as shown in Fig. 3.9b. The time-courses of circadian clocks with internal and external noise inherit the distinctive properties of the circadian clock with internal noise and the circadian clock with external noise.

3.4.2 Critical Coupling

The oscillation frequency $\dot{\theta}^{**}_{\mathrm{m}}$ of a circadian clock with internal and external noise in Eq. 2.13 is assumed to reach steady state when coupling constant K surpasses K^{**}_c. There are two adjustable strengths, one for the internal noise and the other for the external noise. Figure 3.14 shows oscillation frequency of stochastic circadian clock with varying internal and external noise strengths, as a function of coupling constant.

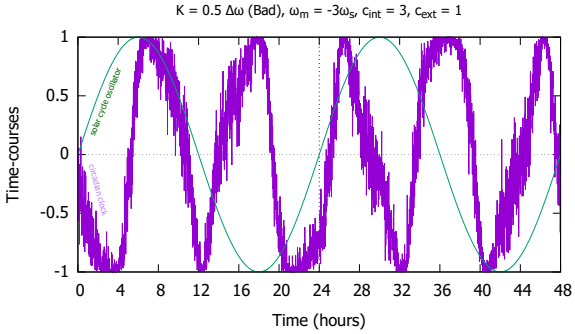

(a) Bad Circadian Clock

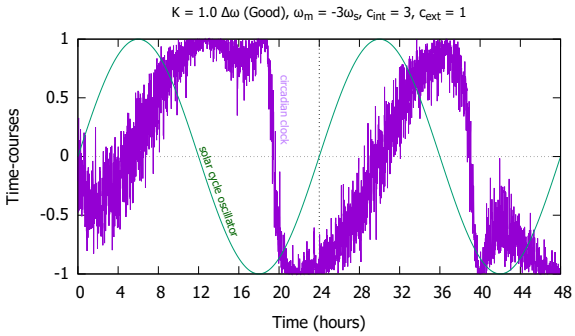

(b) Good Circadian Clock

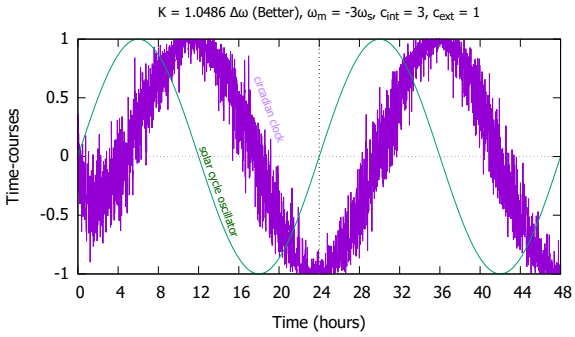

(c) Better Circadian Clock

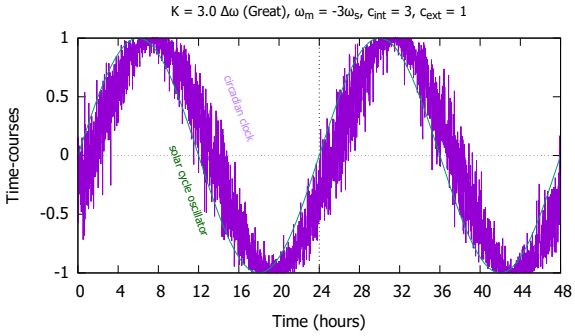

(d) Great Circadian Clock

Figure 3.13: Time-courses of stochastic circadian clocks with internal and external noise computed via Eq. 2.5 and 2.13 with coupling constants: a) $K = 0.5\ \Delta\omega$, b) $K = 1.0\ \Delta\omega$, c) $K = 1.0486\ \Delta\omega$ and d) $K = 3.0\ \Delta\omega$. In all sub-panels, $\omega_{\rm s} = \frac{2\pi}{24}$, $c_{\rm int} = 3.0$, $c_{\rm ext} = 1.0$, $\omega_{\rm m} = -3.0\ \omega_{\rm s}$, $B_{\rm m} = 1$ and $B_{\rm s} = 1$.

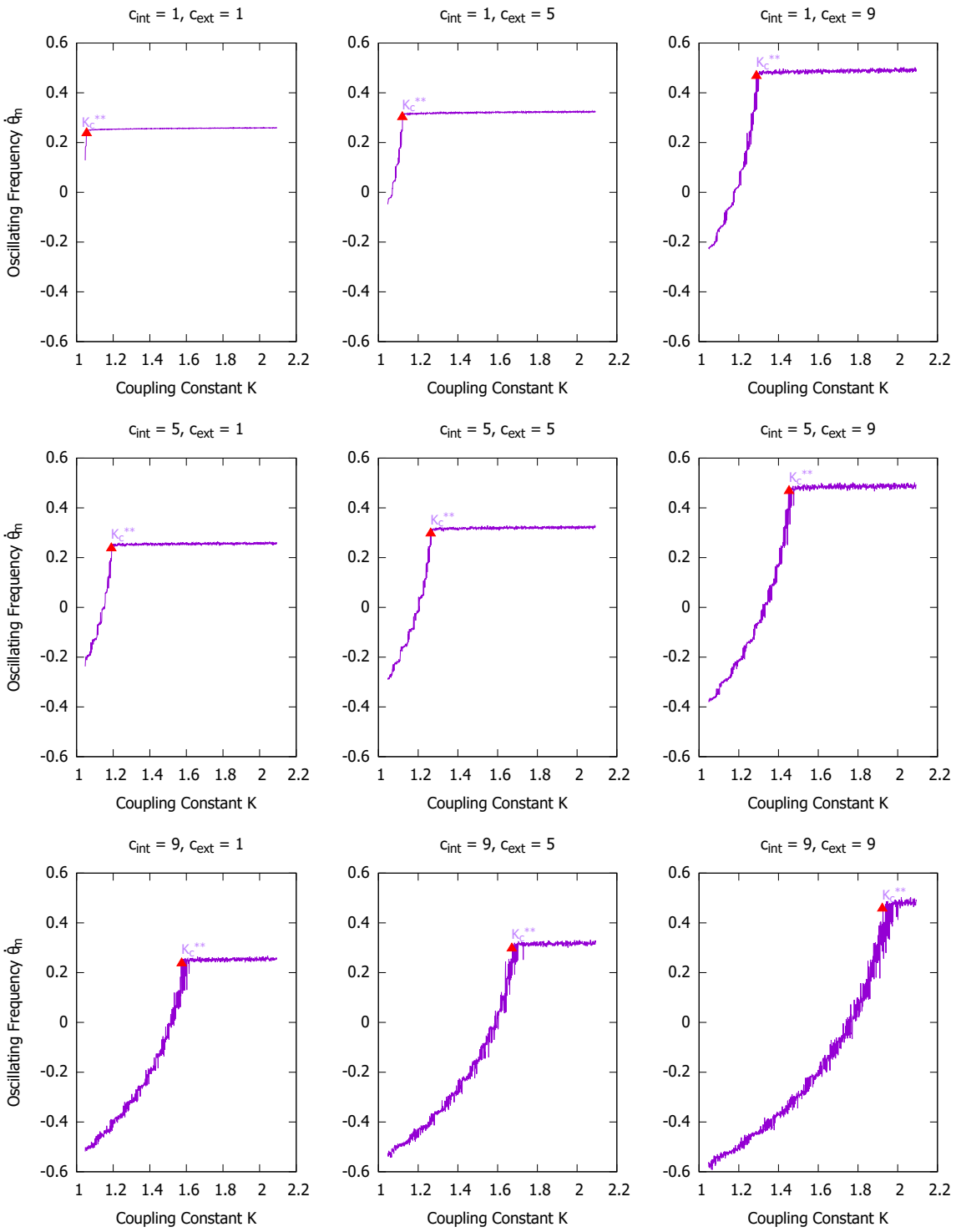

Figure 3.14: Oscillation frequencies $\dot{\theta_{\mathrm{m}}}$ (calculated with Eq. 2.13) of stochastic circadian clock with internal and external noise as a function of coupling constant K. The intrinsic frequency of the circadian clock is set to $\omega_{\mathrm{m}} = -3.0\ \omega_{\mathrm{s}}$. ▲ mark the value of K when $\dot{\theta_{\mathrm{m}}}$ reaches steady state.

A circadian clock with internal and external noise is influenced by the strength of both noises. In the left column of Fig. 3.14, as internal noise strength c_{int} increases (top to bottom), the oscillation frequency reaches to the steady state at about the same magnitude as the solar cycle frequency. Increasing the external noise strength (left to right) increases the steady-state frequency. These properties are distinctive from the stochastic models with either internal or external noise. Incorporating both types of noise. each noise type influences the overall system behavior.

We derive the critical coupling constants (▲ in Fig. 3.14) for the stochastic model with internal and external noise based on the assumption that oscillation frequency of a stochastic circadian clock will relax to steady state about the solar cycle frequency.

Figure 3.15 shows the critical coupling constant K_c^{**} extracted from plots similar to Fig. 3.14, as a function of internal and external noise strength. As for the stochastic model with only external noise, our theoretical derivation does not match the numerical results. The above analysis leads us to conclude that the two types of noise influence the system

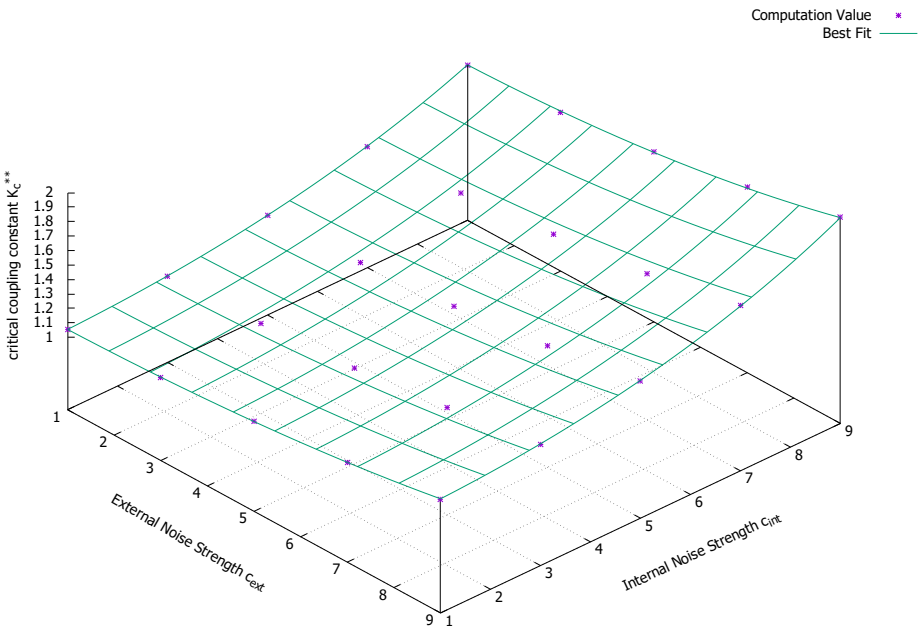

Figure 3.15: Critical coupling constant K_c^{**} as a function of internal and external noise strengths. The numerical result is fit by Eq. 3.2. The fit parameters are $|\Delta\omega| = 1.047$ (rad/hour), $\sigma_{\text{int}} = 0.1002$ (rad/hour) and $\sigma_{\text{ext}} = 0.1005$ (rad).

additively. Hence, we write down the empirical equation to describe the critical coupling constant of a circadian clock with internal and external noise as:

$$K_c^{**} \sim |\Delta\omega| \exp\left[\frac{(c_{\text{ext}}\sigma_{\text{ext}})^2}{4} + \frac{(c_{\text{int}}\sigma_{\text{int}})^2}{2}\right], \tag{3.2}$$

a combination of Eq. 2.48 and 3.1. Fig. 3.15 shows that this hypothesized function fits the numerical data well. The fit parameters in Fig. 3.15 are also similar to the parameters obtained from fitting in Fig. 3.7 and 3.11.

3.4.3 Cost Analysis

Figure 3.16 shows the operational cost of circadian clocks with internal and external noise, which is calculated using the same method as in the previous sections. The operational cost of the four circadian clocks in Fig. 3.13 are explicitly labeled in Fig. 3.16. Figure 3.16 closely resembles Fig. 3.8. For example, both show a non-zero limiting asymptotic cost at large coupling constant (see orange line in Fig. 3.16b), in contrast to the other models we have examined.

Colored dashed lines in Fig. 3.16a represent the critical coupling constants K_c^{**}. The signature of external noise can be seen in the comparison of bright-green and pink lines in Fig. 3.16a, where the pink line has external noise strength $6\times$ the bright-green line. For the case of internal noise, the orange line has internal noise strength $2\times$ the gray line. The critical coupling constant shifts with the internal and external noise strengths. Thus the introduction of internal and external noise increases the operational cost of circadian clocks that achieve frequency synchronization.

If a circadian clock with internal and external noise can achieve frequency synchronization with the solar-cycle oscillator, its operational cost is proportional to the strengths of its perceived internal and external noise, intrinsic frequency, and coupling constant. A circadian clock that will not achieve frequency synchronization will have high operational cost, similar to having no circadian clock regardless of noise strength.

We conclude that operating a circadian clock that doesn't achieve frequency synchronization with the solar-cycle oscillator has similar cost as operating no circadian clock. And based on the result from cost analysis on the stochastic model with internal and external noise, it might not be optimal for a stochastic circadian clock to achieve phase synchronization as well. Since there is a non-zero asymptotic operational cost, the effort of increasing coupling strength can be wasted. A system with larger noise strength will incur higher cost in operating a circadian clock that is frequency synchronized with the solar-cycle oscillator. However, the noise strength does not affect the cost of operating a circadian clock that does not achieve any synchronization, where operating no circadian clock is just as optimal.

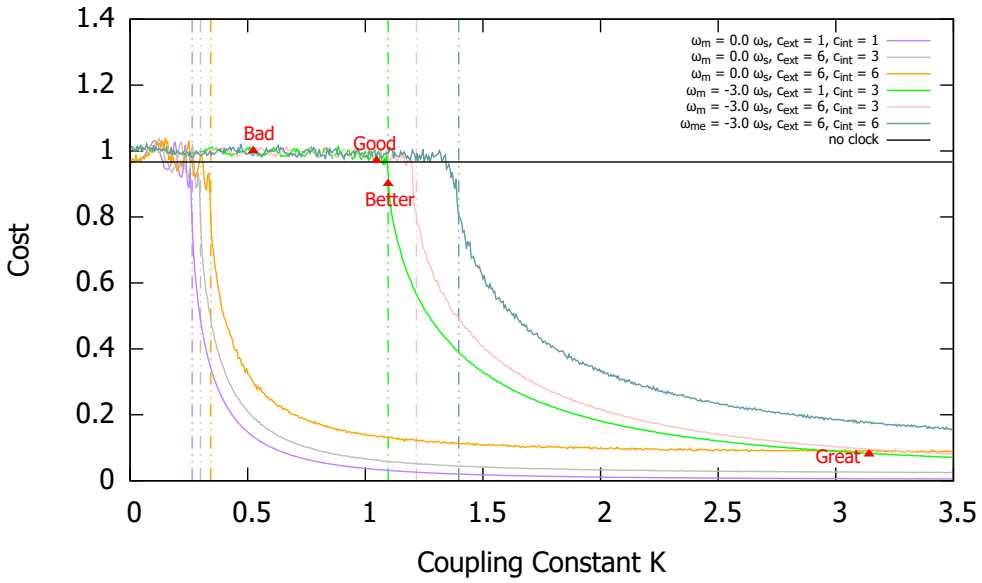

(a) Linear Scale

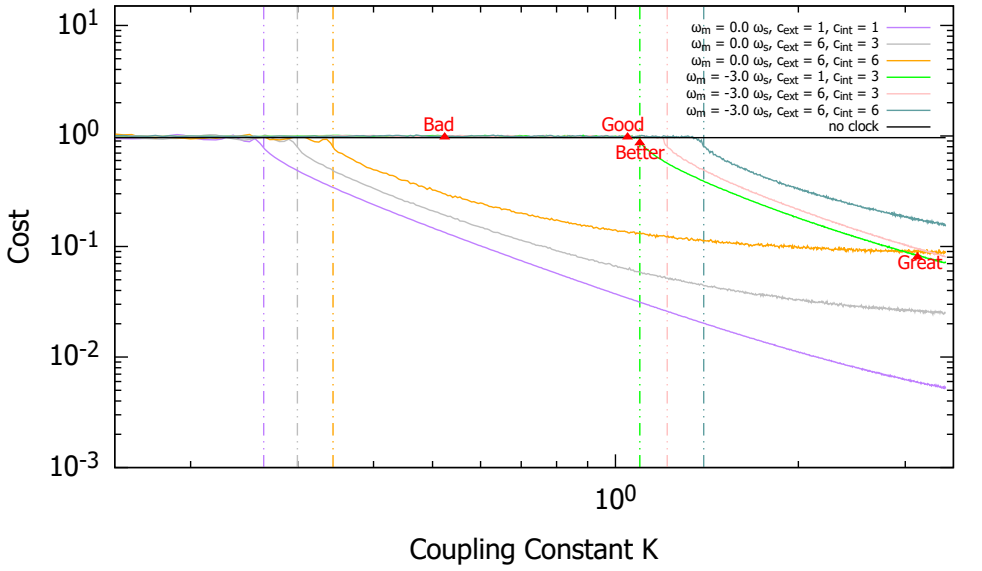

(b) Log Scale

Figure 3.16: Operational cost (Eq. 2.70), averaged over 10 trajectories, as a function of coupling constant for stochastic circadian clocks with internal and external noise. a) Linear scale and b) log scale. ▲ mark the cost of operating circadian clocks shown in Fig. 3.13.

Chapter 4

Conclusion

In this thesis, we have showed the novel possibility of using the Kuramoto model to describe the optimal regulation of a circadian clock. The preliminary results are intuitive. The deterministic model shows that the circadian clock has lower cost of operation when it is frequency- or phase-synchronized with the solar-cycle oscillator. The critical coupling constant depends on the intrinsic frequency mismatch between the two oscillators. For the stochastic model, there is a time-delay effect from the external noise and non-zero asymptotic operational cost from the internal noise. These both lead to higher operational cost for a stochastic circadian clock that when deterministic is synchronized in frequency or phase. The critical coupling constant also depends on the noise strength.

This journey has just begun. The time-delay property from the external noise indeed needs further study. One can imagine there an additional cost associated with achieving a particular coupling constant with the solar-cycle oscillator. Further analysis can be performed on the stochastic model using the Wiener process, which implies solving the Fokker-Planck Equation in Eq. 2.33. Also, we can introduce self-regulation to the model which allows an organism to adjust the coupling status of its circadian clock based on perceived information such as noise strength, cost of operation and cost of coupling, etc.

Bibliography

[1] Nobelprize.org. *"The Nobel Prize in Physiology or Medicine 2017"*. Nobel Media AB 2014. Web. 27 Jul 2018.

[2] Cardoso, F., Cruz, F. D., Silva, D., & Cortez, C. (2009). A simple model for circadian timing by mammals. Brazilian Journal of Medical and Biological Research, 42(1), 122-127.

[3] Sanchez, S. E., & Kay, S. A. (2016). The Plant Circadian Clock: From a Simple Timekeeper to a Complex Developmental Manager. Cold Spring Harbor Perspectives in Biology, 8(12).

[4] Naidoo, N. (2005). Circadian Rhythms in Cyanobacteria. Molecular Biology of Circadian Rhythms, 141-170.

[5] Turek, F. W. (2005). Obesity and Metabolic Syndrome in Circadian Clock Mutant Mice. Science, 308(5724), 1043-1045.

[6] Ebihara, S., Tsuji, K., & Kondo, K. (1978). Strain differences of the mouses free-running circadian rhythm in continuous darkness. Physiology & Behavior, 20(6), 795-799.

[7] Hasegawa, Y., & Arita, M. (2014). Optimal Implementations for Reliable Circadian Clocks. Physical Review Letters, 113(10).

[8] Comet, J., Bernot, G., Das, A., Diener, F., Massot, C., & Cessieux, A. (2012). Simplified Models for the Mammalian Circadian Clock. Procedia Computer Science, 11, 127-138.

[9] Strogatz, Steven H. (2000) From Kuramoto to Crawford: Exploring the Onset of Synchronization in Populations of Coupled Oscillators. Physica D: Nonlinear Phenomena, vol. 143, no. 1-4.

[10] Moore, D., Watts, J. C., Herrig, A., & Jones, T. C. (2016). Exceptionally short-period circadian clock inCyclosa turbinata: Regulation of locomotor and web-building behavior in an orb-weaving spider. Journal of Arachnology, 44(3), 388-396.

[11] Ji, P., Peron, T. K., Rodrigues, F. A., & Kurths, J. (2014). Low-dimensional behavior of Kuramoto model with inertia in complex networks. Scientific Reports, 4(1).

[12] Acebrón, J. A., Bonilla, L. L., Vicente, C. J., Ritort, F., & Spigler, R. (2005). The Kuramoto model: A simple paradigm for synchronization phenomena. Reviews of Modern Physics, 77(1), 137-185.

[13] Sivak, D. A., Chodera, J. D., & Crooks, G. E. (2014). Time Step Rescaling Recovers Continuous-Time Dynamical Properties for Discrete-Time Langevin Integration of Nonequilibrium Systems. The Journal of Physical Chemistry B, 118(24), 6466-6474.

[14] Solak, E., Murray-Smith, R., Leithead, W., Leith, D., & Rasmussen, C. (2002). Derivative observations in Gaussian Process Models of Dynamic Systems. Neural Information Processing (NIPS) Meeting.

[15] Risken, H. (1996). Fokker-Planck Equation. The Fokker-Planck Equation Springer Series in Synergetics, 63-95.

[16] Purves, D., & Williams, S. M. (2001). Neuroscience. 2nd edition. Sinauer Associates.